Appendix D: Solutions to Exercises

THE INTERPRETATION of geological maps and sections is an exercise in visualizing and understanding the complex shapes of rock structures in the subsurface. Developing a good grasp of this subject requires exercises. This book includes a variety of exercises, the solutions to which are listed below. Some exercises require the construction of structure contours on maps or the completion of cross-sections. The graphic solutions are not included here. Thus, students can demonstrate independently how their solutions were obtained.

Chapter one

1-1: a) Well number six in the block diagram of Figure 1-4 has the largest yield. Well number two has the smallest yield. b) The water trapped in the fault zone of well number one comes from the residual soil and fractured granite above it. c) Emplacement of the aplite dike is likely to have fractured the host rock, which may now act as a water reservoir, while the aplite itself is an effective seal rock.

1-2: a) Color the map of Figure 1-7b, as requested. b) The slide mass moved due north down the steepest slope of the terrain after its destabilization by gravity forces. The motion ceased when the mass lost momentum in flat terrain, as can be inferred from the increased spacing of the topographic contours. c) The Old Bierer cabin was covered and destroyed by the 1925 Gross Ventre slide.

Chapter two

2-1: The average slope of the north flank of the volcano in Figure 2-2b is about 20 degrees.

2-2: For example, the geographical coordinates for King Fahd University of Petroleum and Minerals are 26° 19'N latitude and 50° 08'E longitude.

2-3: The map of Figure 2-13 shows a sequence of horizontal layers, labeled O (old) to P (young). a) O is the oldest unit. b) The gravel unit in the stream channels is the youngest deposit. c) The gravel is deposited in stream channels, disconformably cut into the horizontally layered sequence. d) Elevation contours follow the O-S contact at 1,000 meters, S-D contact at 1,100 meters, D-M contact at 1,200 meters, M-P contact at 1,300 meters. e) & f) The highest point is occupied by unit P, located in the center of the map, between 1,300 and 1,400 meters elevation. In fact, this map is from a North American locality, and the letter code stands for a Paleozoic sequence: Ordovician (O), Silurian (S), Devonian (D), Mississippian (M), and Pennsylvanian (P).

2-4: a) All strata in the map of Figure 2-14 are horizontal, because the boundaries of the rock units either coincide with or are parallel to the topographic elevation contours. b) Because all layers are horizontal, specific lithological contacts can be traced at the same elevation everywhere. c) The area below 200 meters in the southeast corner of the map cannot be completed, because it is uncertain whether the conglomerate, exposed elsewhere at 300 meters elevation, extends to this depth. d) The bottom of the conglomerate and the top of the limestone are not exposed. They are the oldest and the youngest units, respectively, outcropping in this area. Only their minimum thickness can be estimated; their total thickness cannot be inferred from the map pattern.

2-5: Construct the cross-section A-B across the map of Figure 2-14 with equal horizontal and vertical rules. Take one centimeter to be one hundred meters. Section A-B crosses two hills, separated by a central valley. The lithological boundaries below the ground surface in the cross-section are all horizontal. The thicknesses of the rock units are from old to young: conglomerate, minimum thickness of 60 meters; coarse-grained sandstone, 150 meters; shale, 50 meters; mudstone, 150 meters; fine-grained sandstone, 100 meters; limestone, minimum thickness of 110 meters. The cross-section should include lithological symbols, a legend, horizontal and vertical scale bars, geographical orientation marked at either end above the section line (together with the letters A and B).

2-6: The columnar section for the stratigraphic units in the map of Figure 2-14 can be quickly abstracted, using their thickness, as already determined in exercise 2-5. The relative resistance to erosion can be indicated by relief in the column, using the common observation that limestone and sandstone are resistant and form cliffs and benches, while mudstone, shale, and conglomerate are less resistant and commonly recede in the relief. Include the vertical scale and appropriate symbols, and write the rock type adjacent to the relief in the columnar section.

Chapter three

3-1: Layer attitudes in Figure 3-7 are: a) For location A: N160E/42SW (clockwise strike/dip), N20W/42SW (counterclockwise strike/dip), and 250/42 (azimuth/dip). b) For location B: N160E/64NE (clockwise strike/dip), N20W/64NE (counterclockwise strike/dip), and 070/64 (azimuth/dip).

3-2: The geological sketch map of Figure 3-7 must include a north arrow, scale bar, approximate lithological boundaries, strike/dip symbols, lithological symbols, and a legend.

3-3: The cross-section of Figure 3-11b shows a layer with an apparent dip of 38 degrees and the apparent thickness is about 1.1 times that seen in the section of Figure 3-11a.

3-4: a) Complete the five sections across the map of Figure 3-12, transferring the lithological boundaries and surface dips from the map to the section, correcting for apparent dip in oblique sections. b) The most representative subsurface structure is seen in section P-Q, normal to strike. It shows a synform and an adjacent antiform. c) Section P-U is the least representative section, because it is taken parallel to the strike of the layers, which appear perfectly horizontal in the section, disguishing their folded nature. Section P-T is, also, misleading, because it shows layers dipping homoclinally northeastward at 10 degrees.

3-5: a) The cheapest pathway for the trench planned across the area of Figure 3-12 connecting P and S cuts normal to strike of the resistant unit C but cuts obliquely through the other units, staying close to the straight line connecting locations P and S. b) The cost saving is calculated by integrating the cost for both alternatives. Following the the more economic pathway, despite it being longer than the straight line between P and S, is about 10 percent cheaper.

3-6: a) The true thickness of layers A, B, and C in Figure 3-17b is 26, 71, and 100 meters respectively. b) A cross-section at 45 degrees to strike of layers A, B, and C, shows them with apparent dips of 11, 35, and 90 degrees. Their thicknesses, also, appear as apparent thicknesses of 26, 85, and 155 meters, respectively.

3-7: a) The cross-section A-B across the map of Figure 3-18 shows a sequence of uniformly, shallowly dipping strata. The lithological symbols should be ruled parallel to the dipping boundary, not horizontal as is sometimes done by novices. b) The columnar section can be constructed with a vertical scale exaggerated, if preferred. The Lower Greensand, Gault, and Upper Greensand units have true thicknesses of 42, 11 and 5 meters, respectively. c) The difference between the true thickness and the layer width appearing on the map is rather large, due to the small dip of the layers. The true thickness is only nine percent of the outcrop width exposed at the surface.

3-8: The true thickness of the aquifer described is 285 meters.

Chapter four

4-1: To complete the section of Figure 4-4c choose symbols given in Figure 2-16.

4-2: The sections across the four different maps of Figure 4-12a to d show: a) A southward sloping ground surface with horizontal layers in the subsurface. b) A gently west sloping ground surface with a vertical dike in the subsurface. c) A gently south sloping ground surface with a homoclinally north-dipping sandstone bed. d) An assumedly flat terrain with an asymmetric synformal fold closure, cut perpendicular to strike.

4-3: The seismic section of Figure 4-9a shows an overall, vertical exaggeration of approximately 1.6 times.

4-4: The true thickness of the aquifer in Figure 4-12a is 21.3 meters.

4-5: The true dip at the base of the Silurian in the Michigan Basin of Figure 4-15 is less than one degree.

4-6: The true dip of the base of the cover sequence of the Arabian shield in Figure 4-16 is approximately one degree. b) The cross-section of Figure 4-16 includes all of the visual distortions, outlined in section 4-3.

4-7: Canyon wall exercise. No map provided. a) The apparent dip is 50 degrees. b) The true thickness is 100 meters. c) The outcrop width is 116 meters. d) The apparent thickness is 255 meters.

4-8: The Paleozoic layers in the Grand Canyon viewed from Lipan Point in Figure 4-19 are cut parallel to strike in the right part of the picture, therefore, all the layers appear horizontal and concordant. However, in the left part of the picture, layers are cut normal to their trend and the angular unconformity between them is obvious. b) Apparent thickness changes are negligible for layers of shallow dip (see Table 4-2).

Chapter five

5-1: a) The average slope of the Precambrian basement of the northeastern Arabian Peninsula of Figure 5-3 is about one degrees. b) The corresponding azimuth/dip varies between 045/01 and 062/01.

5-2: For the structure-contour maps in Figure 5-6a and b: a) Azimuth/dip in location 1 is: 090/40; location 2: 135/35; location 3: 135/65; location 4: 135/35. b) Cross-section A-B shows a surface dipping uniformly, 40 degrees toward the east. Cross-section C-D illustrates a surface that dips southeasterly at 35, 65, and 35 degrees. c) This is a tilted monocline with sharply defined hinges (see chapter seven).

5-3: On the map of Figure 5-7a, the color notation for gold-bearing deposits should appear only on the area outside the horseshoe-shaped enclosure, outlined by the limestone bed. In the cross-section of Figure 5-7b, the area between limestone bed and ground surface should be colored.

5-4: The azimuth/dip of the coal bed on the map of Figure 5-9 is 090/29. b) The cross-section has horizontal and vertical scales equal and shows the ground surface in topographic profile and coal bed in the subsurface, dipping uniformly toward the east at 29 degrees. c) On the map of Figure 5-9, the area west of the outlined coal exposure contains no coal in the subsurface.

5-5:a) The structure contours for the top and bottom of the sandstone formation in Figure 5-11a coincide and trend N-S. b) The vertical thickness of the sandstone bed follows from the difference in elevation between coinciding structure contours: 300 feet. c) The azimuth/dip of the formation is 090/21. d) The true thickness of the formation is 260 feet. e) The ground surface can be outlined in the cross-section, using the elevation contours on the map. f) The entire area between the two sandstone outcrops is not underlaid by the sandstone and is, therefore, colored on the map.

5-6:a) The V-rule suggests the sandstone formation on the map of Figure 5-13 dips southeasterly. b) Use different colors for the two sets of structure contours, thus distinguishing the contours for the bottom and top of the bed. c) The azimuth/dip is 120/38. d) The cross-section shows the ground surface and the attitude and thickness of the sandstone formation in the subsurface.

5-7: a) The structure contours, for the map of Figure 5-14, trend E-W. The azimuth/dip of the sandstone unit is 180/10. b) Vertical thickness of the sandstone unit, inferred from the structure contours, is 300 meters. The true thickness is 295 meters. c) The area north of the sandstone outcrop is not underlaid by sandstone.

5-8: a) The V-rule suggests that all the stratigraphic units on the map of Figure 5-15 dip due west, so that the youngest bed is the (second) sandstone unit above the mudstone. b) Structure contours indicate that the azimuth/dip of all units is 270/22. c) The vertical thickness of the limestone and shale units is 100 meters; their true thickness is 92 meters. The vertical thickness of the mudstone unit is 200 meters; its true thickness is 185 meters. The columnar section represents these thicknesses and reads from old to young: older sandstone, limestone, shale, mudstone, and younger sandstone. d) Section A-B illustrates a homoclinal sequence, dipping wesetrly at 22°. Section C-D shows the stratigraphy apparently horizontal, because it is taken parallel to strike.

Chapter six

6-1: a) The inliers on the map of Figure 6-2 occur below the 500-meter elevation contour. Outliers occur above the 800-meter contour in the northern part of the map and above 700 meters in the southern part of the map. b) The columnar section shows a scaled drill hole section. The relative thicknesses of the horizontal layers can be estimated from elevation differences in the map.

6-2: a) The beds in the map in Figure 6-3 have azimuth/ dip: 090/11. b) The cross-section Y-Z shows a ground surface, outlining a gentle hill with an adjacent valley. The subsurface comprises concordant layers uniformally inclined to the east at 11 degrees. c) The vertical thickness for these gently inclined layers is almost identical to their true thickness: A: thickness unknown, as the bottom of this unit is not exposed; B: 150 meters; C: 100 meters; D: 100 meters; E: 50 meters; F: thickness unknown, as the top of this unit is not exposed. d) The triangular outcrop of unit B is an inlier. The circular outcrop of unit E is an outlier.

6-3: a) The coal outcrop on the map of Figure 6-5 can be traced across intersections of topographic contours and structure contours at the same elevations. b) The azimuth/dip is 150/30. c) Rocks overlie the coal bed outside the ellipse-shaped area, outlined by the coal outcrop at the surface.

6-4: a) On the map of Figure 6-6, the structure contour for 1000 meters is a straight line through points B and C. The structure contour of 900 meters is parallel to line BC and contains point A. Intermediate contours for 25-meter spacing are all mutually subparallel and occur at proportionally spaced distances. b) The base of the sandstone formation can be traced across the map, adding topography contours of 25-meter spacing and marking their intersections with structure contours of corresponding elevation. c) No, the sandstone is not found at location D. d) Cross-section X-Y shows a ground surface,outlining a valley and adjacent hillsides, with a sandstone formation in the subsurface, uniformly inclined to the north at about 20 degrees.

6-5: Completion of the map of Figure 6-7 requires the construction of structure contours at 50 meters spacing and interpolation of topographic contours with similar spacing.

6-6: The limestone bed in Figure 6-8 has azimuth/dip: 203/23.

6-7: a) The azimuth/dip of the coal bed on the map of Figure 6-10 is 180/34. b) The coal outcrop on the map of Figure 6-10 can be traced across intersections of topographic contours and structure contours at the same elevations. c) At location D, you have to drill 100 meters deep to reach the coal seam.

6-8: a) The azimuth/dip of the coal sea on the map of Figure 6-11: 227/27. b) & c) The coal outcrop on the map of Figure 6-11 can be traced across intersections of topographic contours and structure contours at the same elevations.

6-9: a) The azimuth/dip of the bed on the map of Figure 6-12: 130/37. b) & c) The coal outcrop on the map of Figure 6-12 can be traced across intersections of topographic contours and structure contours at the same elevations. d) Choose your colors at convenience.

6-10: Bore hole exercise. No map provided. The azimuth/dip of the sandstone unit is 220/38. The vertical thickness is 200 feet. The true thickness is 157 feet.

Chapter seven

7-1: The structural elements of the folds in Figure 7-1 can be named, following the definition given in the text.

7-2: Exercises on Figure 7-2. a) This is a tricky question, because chevron folds fullfill the requirements of both similar and parallel folds. b) The limestone bed is not a parallel fold, but a similar fold. c) Such folds would be somewhat disharmonic.

7-3: a) The folds of Figure 7-1 and 7-4a and b all are examples of tight folds. Some of the smaller parasitic folds in Figure 4-4a are isoclinal. b) This is a tricky question. An important characteristic of similar folds is that both the wavelength and the amplitude are constant for all layers in the fold. Therefore, none of the folded layers in Figure 7-4b has the largest wavelength or amplitude.

7-4: No map provided. The fold described is commonly asymmetric.

7-5: No map provided. a) Drawing of an antiform with younger rocks in the core. This antiform is not an anticline. b) Drawing of a synform with older rocks in the core. Such a synform is not a syncline. Such folds occur in the lower limb of large-scale recumbent folds (see section 7-6) when refolded into antiformal and synformal closures with upright axial planes.

7-6: The geological maps for the area viewed in the block diagram of Figure 7-10 must include a north arrow, scale bar, approximate lithological boundaries, lithological symbols, strike/dip symbols, axial plane traces, and a legend.

7-7: a) The traces of the axial planes, in the block diagram of Figure 7-16, trend N-S. b) The dip of the fold limbs can be inferred, using the V-rule, where beds are intersected by the drainage channels. The map contains two antiformal closures, separated by a synformal closure. c) All the folds plunge toward the north. d) The section normal to the strike shows the fold structure. The section parallel to the strike shows layers dipping uniformly toward the north, parallel to the plunge of the fold hinge. e) The oldest rocks are found in the core of the antiformal closures, assuming the antiforms are anticlines, too.

7-8: a) to c) The transparency of the photograph in Figure 7-17 cannot show a map, because the aerial view is oblique. What must be sketched is a panoramic view of the landscape. Indicate the major plunging anticline of Sheep Mountain, the dip direction of the layers, and the smaller syncline in the lower corner of the picture. The area exposes a sequence of sedimentary rocks, deformed into open plunging folds with upright axial planes. The more resistant beds form ridges in the landscape. The youngest rocks of the area occur in the core of the small syncline adjacent to Sheep Mountain.

7-9: a) Section A-A', across the map of Figure 7-18, shows a flat ground surface and an open asymmetric synformal closure in the subsurface. Section B-B' shows a similar structure but with shallower dip, due to the oblique angle between the section line and the trend of the structure. The transferral of the map data for the northern limb requires correction for apparent dip. b) Color the layers to classify the map pattern and section. c) The fold plunges at an average of ten degrees toward the north-west. d) The plunge/trend of the fold hinge ranges between 10/305 and 20/305.

7-10: The satellite image, of Figure 7-21 of the Fars platform in the Zagros Mountains, contains numerous doubly-plunging antiforms of the Tertiary Asmari limestone, breached by plugs of infracambrian Hormuz salt. The salt creeps down the flanks of the anticlines in salt glaciers or namakiers. Include a north arrow, scale bar, approximate lithological boundaries strike/dip symbols, lithological symbols, and a legend.

7-11: The dip direction of the fold limbs in the radar image of Figure 7-23 can be inferred where they are intersected by stream channels. The map pattern suggests that the folds are tight to isoclinal, but this is a cutting effect. Most folds plunge very gently, so that their limbs tend to be subparallel in map view, even in open folds. Include a north arrow, scale bar, approximate lithological boundaries, lithological symbols, strike/dip symbols, axial plane traces, and a legend.

7-12: No map provided. Your drawing shows a recumbent fold, or fold nappe, with a stratigraphy that is mirrored about the horizontal axial surface and upside-down on the inverted, lower limb of the fold.

Chapter eight

8-1: Structure contours for fifty-meter intervals can be interpolated on the map of Figure 8-1 between existing contours, using their spacing and the additional points of known elevation. The best prospect for a good hydrocarbon trap is below the NE-SW trending a-nticlinal ridge, particularly near its 960 meter culmination.

8-2: The form lines on the map of Figure 8-4 must everywhere be parallel to or tangential to the trend of the outlined form surface. An attempt can be made to convert this map into a structure-contour map by using the dip to estimate the elevation of form lines, adjacent to the 5000 foot structure contour.

8-3: a) The form lines of the sedimentary beds of the seismocrop map of Figure 8-5 are quite well-outlined by the black curves on the seismocrop map. These form lines enclose depressions, that formed while the adjacent salt stocks rose upward. The diffuse seismic signature of the salt masses precludes the drawing of form lines within them. b) A cross-section across the seismocrop map shows diapiric salt stocks and pillows, separated by mini-basins of layered sedimentary rocks.

8-4: a) The attitude of the limbs of the folded surface, portrayed in the structure map of Figure 8-6a, are: 315/45 and 135/45. It shows a symmetric chevron fold with vertical, upright axial plane and horizontal hinge line. The attitudes of the limbs in Figure 8-6b are: 315/45 and 135/60. It is an asymmetric chevron fold with a horizontal hinge line with an axial plane inclined towards the northeast (if bisecting the inter-limb angle). b) There is no information about the level of the ground surface. The shape of the single surface outlined by the structure contours of Figure 6a shows in a cross-section: A symmetric, upward-closing chevron fold with both limbs dipping at 45 degrees in opposite directions. The section across Figure 8-6b shows an other, asymmetric, anticlinal chevron fold with the NW limb dipping at 45 degrees and the SE limb dipping at 60 degrees. Both folds have narrow hinges.

8-5: The plunge/trend of the fold hinge line outlined - by the structure contours of Figure 8-7b is 51/195.

8-6: a) The axial plane trace of the fold in Figure 8-8a trends N-S, and the hinge line of this synform plunges toward the south. The axial plane trace of the fold in Figure 8-8b trends NW-SE, and the hinge line of this antiform plunges northwestward. b) Figure 8-8a: 21/184; Figure 8-8b: 41/323. c) There is no information about the level of the ground surface. Only the shape of the folded surface can be outlined. A symmetric synform is seen in section G-H. An asymmetric antiform appears in section K-L.

8-7: a) The difficulty is to decide whether structure contours on the map problem of Figure 8-11 should be straight lines connecting *ab* and *cd* or *bm* and *cm*. The lines through *ab* and *cd* would not be strictly parallel. Consequently, these are less likely to be the correct contours. The alternative solution of structure contours with E-W trends is correct. The coal seam turns out to be folded into an antiformal closure about E-W trending axis. b) The coal is further exposed at the surface in the eastern part of the map as follows from intersections between the structure lines and topographic contours. c) The coal layer occurs at 100 meters depth below surface point P. d) The entire area outside the core of the antiformal closure is underlaid by the coal bed.

8-8: Both maps of Figure 8-12a and b are tricky, because the map patterns are suggestive of fold structures. However, both maps represent homoclinal beds, as follows from the construction of structure contour lines. The topographic relief for both maps is identical, but the bed on the map of Figure 8-12a has a shallower dip (010/20) than that of the bed in Figure 8-12b (350/32).

8-9: a) On the map of Figure 8-13, the structure contour of opposite limbs intersect in a herring-bone pattern. The horizontal spacing of the contours on the eastern limb is narrower than that of the western limb. Consequently, the eastern limb (295/48)) dips more steeply than the western limb (080/29). b) The hinge line of the fold plunges northeasterly at 12/015. c) The structure seen is that of a northeasterly-plunging synform.

8-10: a) On the map of Figure 8-15, structure contours remain parallel only if intersection points of the outcrop pattern and topographic contours are connected by N-S-trending lines, as opposed to E-W-trending ones, which are incorrect. b) The layers strike N-S everywhere, even where the outcrop pattern of fold limbs appears curved on the map. c) The axial plane traces occur in a synformal closure occupying the western part of the map and in an antiformal closure occupying the eastern half. d) Both folds have horizontal fold axes and upright axial planes, because structure contours are mutually parallel everywhere and equally spaced. The limbs are straight, so they are chevron folds. e) All strike lines are N-S and alternating limbs dip 30 degrees in opposite directions. f) Cross-section X-Y is normal to the trace of the folds and shows the relief of the ground surface, which slopes gently eastward. The surface of the section is occupied by an open antiform and an adjacent open synform, both with vertical axial planes.

8-11: a) On the map of Figure 8-17, it is more practical to draw structure contours only for the boundaries of units A and H. All structure contours trend N-S. Both units host fold closures. The dips of the layers on individual limbs are constant (20° and 50°, resp.), because the spacing of the structure contours on the fold limbs is constant for each layer. However, all limbs dip eastward and are part of overturned folds. The fold hinges are horizontal, the axial plane dips 35 degrees eastward. The folds are tight chevron folds. b) Two axial plane traces should appear on the map, and both are curved. A north-south trending, concave-east curve can be traced between the two limbs, outlined by unit C and through the fold hinges reflected in the outcrops pattern of the two exposures of unit A. This is the synformal axial plane trace. Another axial trace should be drawn farther eastward, separating the two limbs of formation G and bending similarly as the one explained previously. This is an antiformal axial plane trace. c) Bed H is an inlier, because it is surrounded by younger beds. d) The hinge lines of the folds are horizontal, because all structure contours are subparallel and the herring-bone pattern, typical for plunging folds, is not seen. e) The axial planes dip eastward. f) The cross-section illustrates a gently eastward-sloping ground surface, below which occurs one overturned synformal and one antiformal chevron fold.

Chapter nine

9-1: On the map of Figure 9-3, the outline of the Quaternary deposit of the Duff River corresponds to an unconformity surface. Each of the subparallel coal seams may have been discontinuous, even before folding, if unconformably deposited into separate depressions or if partly eroded and unconformably overlaid by shale. In the latter case, unconformity surfaces may be traced, following the top of the coal layers and across their separation below the Duff River.

9-2: The sections of Figures 9-5b and 9-8b can be completed, using the instructions of chapter four. The transferral of map data to the section line is relatively straightforward. Correction for apparent dip is not necessary for layers of shallow dip, cut here at a large angle to their strike. The unconformity surface below the Kenley grit dips similarly to the beds above it. The sandstone bed should appear in the section below the unconformity surface.

9-3: On the map of Figure 9-9, the Fort Union Formation and Wasatch Formations are mostly conformable, but the base of the Fort Union Formation is a distinct angular unconformity surface. The disconformity surface below the Quaternary gravels is a third unconformity in the Meeteetse area. The Wasatch and Fort Union Formations were subhorizontal after deposition and were tilted about an axis trending N10W effectively to cause the structural strike in that direction with an east dip at 4 to 10 degrees. Earlier, the Mesaverde, Meeteetse, and Lance Formations have been tilted together about a NE-SW-trending axis, that tilted the formations to dip gently toward the SE.

9-4: a) On the map of Figure 9-10, an unconformity surface occurs at the base of unit Y. b) The strata above the angular unconformity dip gently due north with an azimuth/dip of 000/08. c) Beds below the unconformity dip gently toward the westnorthwest with azimuth/dip of 290/11. d) The unconformity surface dips similarly to the overlying strata. e) The sequence of the beds, from old to young, is: L: conglomerate; M: sandy shale; - coal seam -; N: fine-grained sandstone; O: shale; P: coarse-grained sandstone; Y: mudstone; Z: limestone.

9-5: a) Concerning the coal seam on the map of Figure 9-10: Location A, 600 m high itself, is cut by the coal structure contour of 150 m. The unconformity surface is at 450 m. Concludingly, coal is found in bore hole A at 450 m below the ground surface. Location B, 500 m high itself, is cut by the coal structure contour of 300 m. Henceforth, coal is found in bore hole B at 200 m below the ground surface. Location C, 550 m high itself, is cut by the coal structure contour of 400 m. Coal is not found in bore hole C, because the unconformity surface occurs just a little below 400 m elevation in bore hole C. b) The coal seam is missing in borehole C, because it has been eroded away before the deposition of unit Y.

9-6: a) On the map of Figure 9-12, an angular unconformity occurs at the base of unit X. b) The strata above the unconformity surface dip gently toward the NNE with an azimuth /dip of 020/05. c) Unit A is exposed in an inlier; unit X is an outlier where surrounded by unit E. Unit E rests on underlying units and, therefore, would be an inlier itself were it not for the presence of the unconformable unit X. d) Beds below the unconformity are folded about horizontal N-S trending axes. The limbs dip at 17 degrees in opposite directions. Inlier A is in the core of an eroded antiform. Unit E occurs in the core of an eroded synform. e) Cross-section P-Q shows the relief of the ground surface, the angular unconformity surface with an apparent horizontal dip, and the symmetric fold structures farther below. f) The stratigraphic sequence is: A, B, C, D, E, - angular unconformity -, X, and Y.

9-7: No map provided. The isochore map shows contours, trending NE-SW, with spacing progressively diminishing in the southeasterly corner, where the reservoir thickness increases significantly.

9-8: a) On the map of Figure 9-18, the Cretaceous sequence is more than five-kilometer thick in the core of the graben, except for a local circular depression along its axis, where the thickness is less than four kilometers. b) The progressive thinning toward the margins of the central graben suggest that the deposition of the Cretaceous sequence was syntectonic. c) The isopach map shows only the thickness of the Cretaceous sequence and yields no information on its absolute depth.

Chapter ten

10-1: The construction requested for Figure 10-3 is similar to that shown in Figure 10-2b.

10-2: The construction requested for Figure 10-6 is similar to that shown in Figure 10-4.

10-3: There are many different ways in which the parallel perspective of Figure 10-1 can be transformed into an angular perspective diagram. Choose any of the possibilities shown in Figure 10-5.

10-4: a) To complete the isometric projection of Figure 10-9b, draw first, onto the map of Figure 10-9a, a grid spaced similarly to that seen on the top surface of Figure 10-9b. Next, transfer the surface geology at grid-line crossings from the map to the corresponding points in the block diagram. The outcrop pattern is further completed by sketching curves between the transferred data points. b) The geology in the vertical walls of the block diagram use the surface data to infer the most likely subsurface structure. Both sections should be identical but are visually distorted by the isometric projection, each in a different way. c) A practical coordinate system is chosen parallel to the edges of the block, using length units corresponding to those used on the original surface map. The origin of the coordinate system is fixed best in one of the corners of the block diagram.

10-5: a) The block diagram of Figure 10-13 is constructed by first elevating topographic contours from the map in Figure 10-13d to elevated contours, according to the instructions illustrated in Figures 10-12a to f. b) The surface geology is transferred from the map of Figure 10-13d to the elevated-contour block diagram by extrapolation. The two sections P-Q and R-Q are slightly distorted to fit with the squinted vertical walls of the block diagram.

Chapter eleven

11-1: a) The extension in Figure 11-3 between points A and B has a stretch of 1.04. It involves crustal extension of 4 percent. b) The extension in Figure 11-4 between points C and D has a stretch of 1.08. It involves a horizontal extension of 8 percent. It is worth noting that the amount of stretch and extension estimated varies with the choice of reference points (i.e., A and B, C and D). But the extension estimates made here emphasize that normal faults commonly accommodate crustal extension.

11-2: The crustal shortening, in Figure 11-6 between points E and F, has a stretch of 0.88. It involves a horizontal shortening of 12 percent. Reverse faults help to accommodate crustal shortening.

11-3: The minimum displacement of the rock units in the nappe sheet of Figure 11-7b can be inferred from the maximum distance between a fenster and a klippe. That distance suggests a minimum displacement of several kilometers for the thrust unit of Figure 11-7b.

11-4: a) The Alpine fault of Figure 11-10 is a right-lateral wrench fault. b) Right-lateral or dextral or clockwise. c) The transform fault at the spreading ridge of Figure 11-10 shows left-lateral apparent off-set. d) Left-lateral or sinistral or counterclockwise.

11-5: a) & b) To fault the layers in the map of Figure 11-14, use the same principles as shown for the reverse fault in Figure 11-13. If equal off-sets are chosen for the east dipping and west-dipping reverse faults, both maps will look identical. This exercise demonstrates that it is difficult to determine the type of faulting if only a surface map is available. In such cases, further information on the direction of dip of the fault is required in order to distinguish whether the fault is of normal or reverse type.

11-6: Most students, who consider fault movement and its effect on map appearance an easy topic, become intrigued by the unexpected complexity of this exercise in Figure 11-16. Draw the solution in perspective diagrams for three stages (prefaulting, post-faulting, and post-erosional). a) A reverse fault, dipping easterly more steeply than the layers, will cause a stratigraphic repetition. b) A westerly-dipping reverse fault causes a stratigraphic gap in the sequence. These two results for reverse faults are complementary to the effects of normal faulting, illustrated in Figures 1-15a and b.

11-7: a) Cross-section A-B, across the map of Figure 11-17, illustrates three subparallel normal faults (assume an eastward dip of about 60 degrees), that caused a repetition of the stratigraphy. The principle is similar to that illustrated in the sequence of block diagrams of Figure 11-15a. The eastern part of the section is unconformably covered by a limestone unit of shallow dip. Complete the subsurface structure below the limestone, as much as possible, by transferring data from the southern basement outcrop to the section line. b) A brief tectonic history, that explains the map pattern is as follows: A basement sequence of planparallel strata has apparently been tilted by block rotation. The tilted sequence was subsequently cut by three, ESE dipping normal faults associated with an episode of crustal extension in ESE-WNW direction. This episode of extension, commonly associated with basin subsidence, was followed by a regression (due to either a local tectonic uplift or global eustatic sea-level drop). The regression exposed the block-faulted basement units in a land surface, that eroded into a peneplain. Subsequently, the limestone unit was deposited by transgression over a low-relief surface. The transgression could be due to either local tectonic subsidence or global sea-level rise at the end of a glacial. Finally, renewed regression exposed the land surface once again and, possibly, has eroded away parts of the overlying limestone, so that the angular unconformity surface and basement units are exposed anew.

11-8: The construction requested to explain the map pattern of Figure 11-20 is similar to that shown in Figure 11-19, except that the vertical slip is now much larger. Consequently, the intersection line of the two rock units in the west block is below the ground surface, while it would be above the ground surface in the east block, were it not removed by erosion.

11-9: a) The transverse fault in Figure 11-21a has no dip indicated. In such cases, assume the fault surface to be subvertical. The map pattern implies that the east wall of the fault has dropped down relative to the west wall (similar to that seen in the sequence of block diagrams of Figure 11-18a). Erosion leveled the ground surface, and the marine regression implied by the erosion was followed by a marine transgression to deposit the new limestone unit. Finally, renewed regression exposed the angular unconformity on the land surface. b) Cross-section A-B across the map of Figure 11-21a shows all basement units as apparently horizontal, because the section is parallel to strike. The western block is uplifted relative to the eastern block. The eastern basement block is unconformably overlaid by the limestone unit.

11-10: a) The map of Figure 11-22 illustrates strata, homoclinally dipping toward the SSE. A central fault block has dropped, relative to the wall rock at either side. The subsided structure is a graben, and, therefore, the two faults are most plausibly interpreted as inward-dipping, normal faults. Such faults record a period of extension. Although the same map pattern could alternatively be explained by two outward-dipping, reverse faults, such reverse faults of opposite dip are extremely rare and, therefore, are less likely. b) Cross-section C-D shows subhorizontal strata at the same elevation in the west and east block. The central fault block has dropped, and the amount of displacement can be determined, projecting the boundaries of the strata on the map to the appropriate depth in section C-D, using the 30-degree surface dip.

11-11: For the map of Figure 11-23, the assumption of dip-slip faulting and exclusion of strike-slip faulting is reasonable. Field studies have shown that closely spaced faults, separating correlatable rock strata, are more likely to be dip-slip faults, rather than strike-slip faults. The latter faults commonly occur as discrete, individual faults and splay only if displacements are large so that rock units cut by the fault can no longer be found within short distances. a) These are oblique normal faults, formed by E-W extension of the area. The shallow dip of the fault blocks may be due to block rotation coeval with the faulting, rather than prior to the faulting. b) Cross-section E-F shows west-dipping normal faults, separating strata gently dipping toward the east. Displacements follow from the construction.

11-12: No map provided. This is a very simple exercise, but beware that the arrows used are half-arrows, showing relative sense of shear only. These half-arrows differ from full arrows which would be vectorial and wrongly suggest absolute sense of movement. Solutions: a) A sinistral set of strike-slip arrows, showing clockwise sense of shear. b) A dextral set of strike-slip arrows, showing clockwise sense of shear. It is worth noting that the displacement seen on *dip-slip faults* is sometimes referred to in terms of sinistral or dextral sense of shear. How-ever, this terminology is never used by experienced structural geologists for dip-slip falts. They realize that the same dip-slip fault, where cut by a canyon, shows oposite sense of shear on opposite vertical canyon walls. Consequently, the terms sinistral and dextral are unambiguous only for *strike-slip faults*, which can be viewed on horizontal surfaces only and thus have a unique sense of shear.

11-13: The map pattern of Figure 11-25 suggests the presence of a folded sandstone layer to the untrained mind. This interpretation is false, as follows immediately from the construction of structure contours. a) The sandstone formation in the western block dips uniformly to the south with azimuth/dip: 185/18. b) The fault plane is strictly vertical, because it cuts across different elevations without curving on the ground. c) The attitude of the sandstone formation in the eastern block is the same as in the western block, because the spacing of structure contours is the same. d) The dip-separation follows from the vertical elevation difference of laterally-matching structure contours at either side of the fault trace: 50 meters. e) Assuming the dip-separation is entirely due to dip-slip, the eastern block has subsided, relative to the western block. f) The strike-separation follows from the horizontal separation of structure contours of the same elevation at either side of the fault: 200 meters (measured along the fault trace). g) If due to strike-slip alone, the fault is sinistral (or left-lateral or counter-clockwise). It is important to realize that the true sense of fault-slip cannot be inferred without reference points, known previously to be in continuous contact across the fault plane, now separated by fault displacement. However, exercise 12-10 gives an example of a problem where fault-slip can be reconstructed unambiguously.

Chapter twelve

12-1: a) The western part of the map of Figure 12-3a includes a repetition of stratigraphic units in reverse order. This is characteristic for folded sequences. The axial plane trace trends NE-SW between the fold limbs and across the fault line. The single strike/dip symbol on the map helps to decide that the fold closure is a synform, rather than an antiform. The synform is displaced by the faults. The dip of the fault is unknown, so assume it is steep. The displacement of the synformal closure (analogous to that portrayed in the series of block diagrams of Figure 12-12a to c) indicates that the NE block is downthrown with respect to the SW block. If the fault dips NE, it is a normal fault. In contrast, a reverse fault must be concluded if the fault were to dip to the SW. Both interpretations are possible on the basis of the data provided. b) Section A-B shows the faulted synform with apparent dips for the fold limbs, and the west limb is steeper than the east limb, as suggested by the different outcrop widths for either limb on the map. The basement is covered in the east by discontinuous conglomerate units, overlaid by limestone and sandstone. c) A brief geological history: The basement sequence was folded about NE-SW-trending fold axes. Subsequently, it was faulted transversely by a NW-SE-trending dip-slip fault that threw the NE block down relative to the SW block. Subsequently, erosion leveled the ground surface. The conglomerate may be a remnant of a braided river deposit on a coastal plain. A marine transgression deposited limestone and sandstone onto the basement. Marine regression and subsequent erosion of the land surface exposed both the cover and the underlying basement structure, as well as the unconformity surface that separates them.

12-2: a) The triangular area, enclosed by the three faults on the map of Figure 12-4, is downthrown with respect to the east and west walls. The displacement by each of the transverse faults is similar to that portrayed in Figures 12-2a to c. The block to the north of the third, WSW-ENE-trending fault is downthrown with respect to the southern structures. b) The map shows a transversely faulted antiform, plunging ENE, covered by horizontal conglomerate. A longitudinal fault juxtaposes the conglomerate in the north against unit A. The stratigraphic sequence from old to young is: M, R, T, A, - angular unconformity -, O. c) A basement sequence has been deformed by crustal shortening in NNW-SSE direction into a gentle antiform, plunging toward the ENE. A central section of the fold is downthrown between two transverse faults, possibly in a graben structure, bounded by normal faults. (Extension normal to the shortening direction is quite common, and faults transversely across folds are mostly of normal type). The entire structure was leveled by erosion and unconformably covered by a basal conglomerate. The conglomerate is cut by a ENE-WSW-trending fault, which represents the latest geological event recorded in the map area. d) The oldest rocks of unit M are exposed in the core of the antiform. e) The highest part of the plunging antiform, occurring to the east of the two transverse faults, is the best target for hydrocarbon exploration. Upward migrating gas and oil may have accumulated into a reservoir below the fold hinge and are sealed by the N-S-striking fault. An exploration drill hole should be sunk into the fold closure about 100 meters to the NE of the 600-meter high peak.

12-3: a) Repetition of the stratigraphic units in reverse order in the central part of the map of Figure 12-7 indicates that the basement sequence is folded about N-S-trending axes. Both the E-W-striking stream channel and outcrop pattern of the unconformable limestone unit suggest that the central section of the map area is a topographic low. The curvature of the fault, convex toward the east, suggests it dips eastward. The beds to the west of the longitudinal fault dip westward, as indicated by the intersection at the stream channel crossing and by the single strike/dip symbol. This fixes the stratigraphic sequence, so that the sandstone is overlaid by the shale unit. Consequently, the fold structure to the west of the longitudinal fault is a synform. It leans against a faulted antiform in the west, where conglomerate is exposed in the fold core. The more complete stratigraphic section in the west wall of the antiformal structure indicates that the west wall is upthrown relative to the eastwall. This situation is similar to that portrayed in Figure 12-6a to c. b) Cross-section A-B shows the ground surface gently sloping westward. The subsurface structure shows an open antiform in the western part of the section, separated by a normal fault from an open synform in the central part of the section. The basement is unconformably overlaid by a horizontal limestone unit. The conglomerate in the basement can be traced below the limestone cover in the section. Include a legend with the section, placing the units in their appropriate sequence: old below, young above. c) The area was shortened in E-W direction, which led to deformation of the basement units into N-S-trending open folds with upright axial planes and horizontal hinges. If the longitudinal fault were to dip westward, it would be a reverse fault and, thus, could be coeval with the shortening episode, that led to folding. However, the curvature of this fault suggests that it dips eastward, which makes it more likely a normal fault, and the west block was upthrown. The normal fault postdates the folding and may be indicative for crustal relaxation and extension after horizontal shortening. The ground surface of the faulted fold sequence was denudated by erosion and covered by a transgressive limestone unit. A later regression exposed the land surface shown in the map. The maximum elevation of 83 meters indicated on the map, is much greater than the maximum global sea-level drops of about 200 meters recorded in geological history. This knowledge leads to the conclusion that the regression, which exposed this area above sea-level, is mostly due to local tectonic uplift, rather than sea-level changes.

12-4: The map of Figure 12-8 includes two longitudinal faults. One of the faults separates the sandstone from the conglomerate unit in the western part of the map. The other fault occurs between the white marl and limestone units. a) The section shows a flat ground surface, and the subsurface shows a central, gentle, upright, horizontal synform with a core of limestone. Both limbs are longitudinally faulted. Younger units of the faulted limbs lean against older units of the central synform. This indicates that the central section of the map is upthrown. If the faults dip outward, it is a horst structure. If the faults dip inward, it is a pop-up structure with reverse faults, indicative of shortening. Such reverse faults could be formed coeval with the folds of the area. Each of the alternative interpretations could be valid, and no conclusive evidence is given here to rule out either of them. b) The central block moved upward relative to the limbs downthrown at either side of the synformal core.

12-5: a) The map of Figure 12-11 illustrates a transversely faulted, SE-plunging, antiformal fold closure. The rocks in the fold hinge of the SE block are juxtaposed against older rocks in the NW block. The NW block, therefore, must have been upthrown relative to the SE block. This situation is reverse to that illustrated in Figures 12-10a to c, where the block containing the nose of the fold is upthrown instead of being downthrown, as shown here. b) Cross-section A-B shows an apparently asymmetric antiform, but this asymmetry is largely due to the way the section line cuts the fold. The west limb is cut parallel to the strike, and layers on that limb, therefore, appear with a very shallow apparent dip. The NW block is upthrown. Consequently, if the fault surface is drawn dipping southeastward, it would be a normal fault. Conversely, if the fault were to dip northwestward, then it must be a reverse fault. Each of the alternative interpretations could be valid, and no conclusive evidence is given here to rule out either of them.

12-6: a) The map of Figure 12-12 illustrates a SSE plunging synform, displacing a transverse dip-slip fault. The rocks in the fold hinge lean against older rocks in the southern block. The southern block, therefore, must have been upthrown, relative to the northern block. This situation is reverse to that illustrated in Figures 12-9a to c, where the block containing the nose of the fold is upthrown instead of being downthrown, as shown here. The basement fold is unconformably overlaid by a limestone unit in the NE corner of the map area. b) Cross-section A-B shows a southward-sloping ground surface. The basement layers in the subsurface appear with nearly horizontal apparent dips; the northern block is downthrown. The basement in the northern end of the section is covered by a subhorizontal limestone unit. c) This area was deformed by shortening in ENE-WSW direction into a synform fold, plunging south-southeastward. The fold is cut by a transverse fault, the northern block is downthrown. Consequently, if the fault were to dip northwestward, it would be a normal fault. Conversely, if the fault were to dip southeastward, it must be a reverse fault. Each of the alternative interpretations could be valid and no conclusive evidence is given here to rule out either of them.

12-7: a) The area in the map of Figure 12-13 exposes gently folded sedimentary rocks. A western synform adjoins an eastern antiform. Both folds plunge northerly. The two subparallel transverse faults in the central part of the map enclose an upthrown fault block, possibly a horst structure, bounded by outward-dipping normal faults. The transverse fault in the SE corner of the map separates a southeastern block, that was upthrown relative to the northern block. The longitudinal fold cutting the antiform nose in the NE corner of the map has an eastern wall, upthrown relative to the western wall. This dip-slip is opposite to that illustrated in Figures 12-15a to c. b) Cross-section A-B shows a gentle synform in a horst block, sandwiched between a downthrown east-dipping limb in the westernmost block and another east-dipping limb in the easternmost, downthrown block. c) The area, which comprises coal seams, has been folded into gentle synforms and antiforms, plunging northerly. The folds are block-faulted by what are, most likely, transverse normal faults. These faults have accommodated extension, normal to the direction of shortening, indicated by the folds. The longitudinal fault in the NE corner of the map may be an east-dipping reverse fault, formed coeval with the folding event.

12-8: a) The map of Figure 12-16a exposes a doubly plunging synform, displaced by longitudinal normal faults. The axial plane trace trends E-W. Each of the four normal faults has its northern wall upthrown relative to the southern wall. b) Cross-section A-B shows normal faults dipping southward. The southern limb of the synform in the northern end of the section is faulted and repeated three times in the southern part of the section. c) Lavas of "Old Red Sandstone" age are overlaid by Devonian rocks, including sandy mudstone, marl with coal intercalations, and shale. The Devonian sequence was folded into a doubly-plunging synform by N-S-shortening. The folded sequence was then stretched by block-faulting, involving normal faults.

12-9: If the structure on the map of Figure 12-19 were to be a synform, then the southern block was downthrown. But if the structure is an antiform, then the northern block was downthrown instead. The strike-separation indicates a component of dextral strike-slip was, also, involved in the fault movement.

12-10: For Figure 12-19: If it is the type of fold specified in exercise 12-10, the net-slip can be constructed as follows: The strike-slip component, measured between the map projection of the axial plane traces, is 120 meters. The vertical dip-slip component can be determined from the elevation difference between the fold hinge at either side of the fault; it amounts to 210 meters. The amount of net-slip of 242 meters follows from vector addition.

12-11: The map of Figure 12-20a shows a NE-SW trending breccia zone, marking a discontinuity in the outcrop pattern of the strata at either side of the zone. The strike-dip data on the map indicate a gentle antiform is left-laterally displaced by the breccia zone, which, therefore, is a fault zone. Consequently, the breccia must be of tectonic, rather than of sedimentary, origin. The map of Figure 12-20b shows a tight NE-SW-trending synform, left-laterally displaced by a NW-SE-striking fault.

12-12: a) Structure contours for the fault plane on the map of Figure 12-21 indicate its azimuth/dip is 090/34. b) The azimuth/dip of the sandstone layer in the hanging wall is 090/18. c) The fold hinge line in the foot wall, which hosts a synform, trends N-S and is horizontal. d) The west limb of the synform has azimuth/dip: 090/18. The east limb has azimuth/dip: 270/34. e) Cross-section A-B shows an asymmetric synform in the foot wall of a fault and an east-dipping limb in the hanging wall. f) The fault is longitudinal to the fold structure. It is most certainly a reverse fault, that cuts through the hinge zone of an antiform, that occurs east of the synformal closure seen on the map.

Chapter thirteen

13-1: This question requires students to think more independently to search for geological information. Consult your fellow students or instructor for help in finding nearby tectonic settings with modern magmatic activity.

13-2: Ring dikes are igneous intrusions, typically emplaced along conical surfaces, the diameter of which widens downward. The vertical block surrounded by the ring fracture is commonly subsided into a magma chamber. Cross-section M-N across the map of Figure 13-15a shows a ring dike of constant width. This implies that the dip of the ring fault is everywhere equal. The space for the intrusion is created by lowering the central block. Figure 13-15b is a map with discontinuous ring dikes of variable thickness. Cross-section O-P should show a smaller cauldron block, lowered inside a bigger cauldron block. Both blocks are bounded by ring faults, that are subvertical in the east. No dike is formed there, because lowering of the central cauldron block(s) creates no space if walls are subvertical. However, in the western part of the map area, ring fractures dip outward, so that lowering of the cauldron block creates space for the igneous intrusion of ring dikes.

13-3: Cross-section Q-R, across the map of Figure 13-16, illustrates that all the igneous rocks on the map are interconnected in the subsurface and form part of a single pluton. The pluton is intruded into country rock, that made up of a folded sequence. The coal-bearing sandstone unit occupies the core of a synform. The conglomerate is exposed in the eroded cores of antiformal closures, occurring at either side of the central synform.

13-4: Section X-Y, across the map of Figure 13-17, shows dikes A and B are subvertical, as can be inferred from structure-contour rules. The attitude of dikes C and D is more ambiguous, but their straightness suggests they are, also, steep. Although all dikes have the same width at the surface, their apparent thicknesses in the cross-section are all different.

13-5: The igneous complex of Mull, Scotland, in the map of Figure 13-20, hosts an interesting collection of ring dikes. From the cross-cutting relationships in the map patterns, it appears that a suite of earlier acid ring dikes is locally truncated by basic ring dikes. The center of intrusion for both sets of ring dikes is in the southeast of the map. This early set of ring dikes is truncated in turn by the Glenn Cannel granophyre intrusion. The Loch Ba felsite is a late cone sheet, that cuts across all other intrusions.

13-6: The section, across the Anstruther gneiss-dome of Figure 13-6, can, on the basis of the map data, be drawn only in very speculative fashion. The important notion is that the supracrustals are layered volcanoclastics and sedimentary rocks, that are draped, more or less, concordantly around the gneiss-dome.

13-7: The form lines, for the satellite image of Figure 13-27, follow the trend of the layers, discernable in the supracrustals, wrapped around the plutons. The foliation within the plutonic gneiss-domes themselves is less well-defined. The form lines in the supracrustals delineate down-warped dome-and-basin folds (not further treated here; they are complex structures).

Chapter fourteen

14-1: Interpretation of the geological history implied in the section of Figure 14-4: The oldest rocks in the sequence are the basement rocks, which are overlaid by unconformable lake and river deposits. All these rock units are buried by a flood basalt sequence. Each episode of basalt flooding was followed by weathering and erosion, as can be inferred from the incision by stream channels, lake deposits, and fossil soils in the top of each basalt flow. The remains of cinder cones are locally preserved as pyroclastic aggregates near feeder dikes, cutting through older layers of basaltic lava. Subsidence must have occurred after the cessation of the magmatic epoch, so that the postvolcanic succession could accumulate.

14-2: Using the legend of Figure 14-17c, it seems that the lava flows at Kilauea originate from fissures, that slowly propagate laterally from a common point of origin. For example, in 1956, eruption was first observed in location A near Puu Honuaula, after which the fissure eruption propagated norhteastward to B, C, D, E, and F. A little back-tracking took place when renewed eruption occurred at location G between D and E. But the general trend was that of a fissure, propagating from A to P, to vent the Kii flow of 1955. Later that year, a fissure opened further southeastward, venting basalt flows between locations U and Q. In 1960, the northwestern tip of the fissure system reactivated and vented a lava flow near the Kapoho Crater.

14-3: The sections of Figure 14-21b to d suggest that slide masses, involved in the 1980 collapse of Mount St. Helens, moved northward for several kilometers.

14-4: Many more geological hazard maps are still needed. Study the example set by USGS Special Publication L-836.

14-5: The formula for estimating the rock volume involved in the collapse of a volcanic cone is: $V=\pi h^3/[3(\tan\alpha)^2]$. The collapse of a cone 300 m high and sloping 30 degrees involves a rock volume of $85x10^6$ cubic meters.

14-6:The speculative map of the Valles Caldera area, five million years into the future, would probably expose basalts and rhyolitic ring dikes. Fifty million years from now, the entire magma chamber below the caldera floor will be exposed as a subcircular pluton.

Chapter fifteen

15-1: The search for impact structures near your home region requires literature study. Ask your instructor and librarian for references.

15-2: a) Coloring of the slide masses, on the drift map of Figure 15-17a, reveals that the tiny village of Turrillas, Spain, is built on prehistoric landslides. b) The cross-section of Figure 15-17b illustrates a reverse fault (NBF), that has moved a hanging wall of Paleozoic and Mesozoic basement rocks onto a foot wall of Neogene strata. The schist, phyllite, and carbonate rock of the uplifted basement have all supplied material for various landslides, strewn around the northern slope of the Sierra Alhamilla. Cerro Minuto threatens to bury Turrillas village if it follows the slide path of earlier, prehistoric slides, on which the village is built. A device for monitoring movements and ground creep urgently needs to be installed at Cerro Minuto to protect the villagers and their dwellings.

15-3: a) Karst areas are prone to sudden collapse of the ground surface into sinkholes. b) Sinkholes are generally unsuitable for waste disposal, because they are surrounded by porous rocks, that would soak up liquid waste, thus risking contamination of aquifers in the subsurface. Special preparations of the site could reduce the risk of subsurface contamination of waste repositories, hosted in sinkholes.

15-4: The end-moraines deposited during the Illinoisan glacial (550,000 to 400,000 years ago) are less prominently preserved than the those of the Wisconsinian glacial (180,000 to 10,000 years ago). The Wisconsinian end-moraines of Figure 15-23 include various stages, as is evident from the sinuous ridges. What is seen in the map is a pattern of glacial retreat. The youngest end-moraines occur farthest north.

Chapter sixteen

16-1: The frequency of visible light is of the order of 10^{16} Hertz. Thermal infrared waves have frequencies ranging between 10^{16} and 10^{15} Hertz. The frequency of radar waves ranges between 10^{13} and 10^{11} Hertz. For comparison, the frequency of FM radiowaves is of the order of 100 MegaHertz, and the AM radio band occupies frequencies ranging between 531 kHz and 1,602 kHz.

16-2: a) One of the strengths of remote-sensing methods is that they provide instantaneous access to any place in the world. No permission is required to enter the terrain. Cumbersome ground logistics are thus avoided. Remote-sensing images reduce the ground surface to a scale that can be managed and analyzed in desk studies. Conventional aerial photographs are commonly panchromatic and analog, and cover areas of up to one hundred square kilometers in each frame. In contrast, satellite images are multispectral and digital and cover areas of several thousand to ten-thousand square kilometers in each frame. Satellite images can be digitally merged with other databases or even transformed into virtual reality images with three-dimensional perspective of the terrain, but the ground resolution of aerial photographs is still up to a hundred times better than that of any digital satellite image. b) Detailed field investigations by geologists on the ground are costly and time-consuming. Only rocks in their immediate vision can be studied. A synoptic mental picture of the spatial distribution of rock units and structures is obtained only after completing the geological map. Some areas are inaccessible for geological ground personnel, due to political, strategic, logistical, or bad weather limitations. However, the advantage of ground studies over remote-sensing methods is that rock samples and fossil specimens can be identified and, if so required, collected for further study. Mineralization zones and the attitude of structural fabrics can be measured in detail. Also, field geology is a lot of fun!

16-3: Oblique and vertical aerial photographs appeared on the cover of this book and in Figures 1-2a, 1-6a, 1-7a, 1-8a & b, 1-9c, 2-6, 2-8, 2-10, 2-12, 7-17, 7-26, 13-1b, 13-6, 13-11a & b, 13-14, 14-3b, 14-11a, 14-32, 14-34c, 15-10, 15-12, and 15-20a & b. Panoramic photographs taken from ground-based vantage points appeared in Figures 3-1b, 4-19, 7-7a, 7-25a & b, 9-4a, 9-14, 13-4, 14-11b, 14-25, 14-28a, 15-4, 15-9a & b, 15-15, 15-16b, and 15-18. Landsat images were used in Figures 7-21, 13-1a, 13-27, and 15-6b. The photograph of the lunar crater in Figures 15-3a & b were taken from aboard the Apollo spacecraft. A radar image was used in Figure 7-23. Seismic maps were used in Figures 4-9a, 8-5, and 10-8. More remote sensing images appear in chapter sixteen: Figures 16-11 to 16-14 (aerial photographs); Figures 16-19a, 16-23a & b, 16-24a & b, and 16-27b (Landsat); Figure 16-20 (SPOT); Figure 16-27a (Space Shuttle radar); Figure 16-29 (Magellan radar).

16-4: Remember that aerial photographs are commonly printed at a quadrangular format of 22.9 by 22.9 inches. Standard aerial photographs at 1:60,000 scale, therefore, cover an area of 14 by 14 kilometers. Those taken at 1:40,000 cover an area of 9 by 9 kilometers. Aerial photographs of scale 1:30,000 cover 7 by 7 kilometers on the ground in each frame.

16-5: a) The stereopair of Figure 16-11 illustrates an arid landscape, devoid of any vegetation. The area is relatively flat, except for a number of barchanoid dunes, resting on a desertscape. Any drainage pattern is absent. The dominant erosional agent is a northerly wind, as can be inferred from the shape of the barchanoid dunes. Settlements and cultivation centers are absent. b) The stereopair of Figure 16-12 covers an arid area, largely devoid of any vegetation. The landscape is dominated by a series of ridges, formed by resistant bedrock in a folded sequence of sedimentary strata. The flanks or limbs of the folds are transected by parallel stream channels. The drainage network is dry, but its extent suggests that the area is occasionally inundated by torrential rains. The main stream runs roughly from the south toward the north. The map shows a NW-plunging synform in the north of the image. The attitude of the limbs can be inferred by applying the V-rule, where stream channels intersect resistant beds. The folds are gentle to open. Brief geological history: A sedimentary sequence was buried, folded, and uplifted to give rise to the present morphology. c) The stereopair of Figure 16-13 covers an arid landscape. A dendritic drainage pattern runs off to the southeast corner of the photograph. The main wadis are floored by light-toned gravels and lined by trees and shrubs of dark albedo. The region is arid but occasionally receives torrential rains. The bedrock includes a steeply foliated, dark-toned metamorphic belt, trending NW-SE. This metamorphic belt of schists is adjacent to light-toned granitic plutons. The regional structure is transected by NNE-SSW-trending fissures. These fissures form shallow ridges in the landscape. They are, in fact, intruded by basic dikes of dark albedo. One of the fissures shows dextral strike-slip displacement of the metamorphic belt. The sequence of supracrustals, including schists, has been sandwiched between two buoyant plutons. The foliation in the supracrustals is concordant to the boundaries of the adjacent plutons and was formed during their emplacement. The penetrative foliation indicates formation under metamorphic, deeper crustal conditions, perhaps below ten kilometers depth. The fissuring indicates brittle deformation, which commonly occurs only at shallow crustal depths. In fact, the basement is 600 million years old, and the fissures and the basic dike swarm are much younger, only about 30 million years old. d) The stereopair of Figure 16-14 covers an arid landscape. The drainage pattern varies locally from dendritic and trellis on the light-toned basement to radial off the dark-toned plateau of basaltic lava. The region occasionally receives torrential rains. The bedrock below the basalt plateau is made up of E-W-foliated granite or gneiss. The basement is cut by N-S fissures, invaded by basic dikes. These fissures possibly are the conduits that allowed for the extrusion of the flood basalts.

16-6: It takes about nine SPOT images to cover the same area as a Landsat image. Total coverage of the US requires about 4,500 SPOT images.

16-7: The SPOT image of Figure 16-20 covers an arid region. The Draa Plateau hosts a centripetal drainage pattern, that runs off toward the east. The plateau is floored by sedimentary rocks of Carboniferous age. The basal layers of the Carboniferous sequence form ridges in the landscape and are cut by parallel valleys. The shallow basin, made up of gently-dipping Carboniferous beds in the southern part of the image, contrasts with the tightly folded Devonian beds just north of the Draa Valley. Directly to the south of the Draa Valley, one must interpret an E-W-trending fault contact between the Carboniferous and the Devonian sequence. The asymmetry of the folds in the Devonian beds indicates a dextral sense of shear for the Moroccan Border fault.

16-8: The digital pixel map of Figure 16-22a can be converted into a false color image by choosing arbitrary colors for a particular range of digital numbers. The resolution is poor, but the image includes a highway, highlighted by the array of digital numbers between 48 and 56.

16-9: The coloring of Figure 16-28 helps to examine how the distinguished features correspond to the radar image of Figure 1-27a.

Indices

Geographic Index

(Bracketed numbers refer to Figures)

Ad Dhana sand sea, Saudi Arabia 282, (16-27a & b), (16-28)
Aegean Sea, Greece 231, (11-1b), (14-29a)
Afar triangle, Africa 212, (14-8)
African plate 210, (14-8)
African rift valley 212, (14-8)
Agoho village, Camiguin Island, Philippines 228, (14-26)
Akroteri, Crete, Greece 231
Alaska Peninsula 192
Aleutian trench (13-7)
Aleutians 192
Alpine fault, New Zealand 158, 159, (11-10)
Alpine Mountains, New Zealand (11-10)
Alps, Europe 202
Anak Krakatao, Indonesia 232, (14-30b)
Anatolia fault, Turkey (11-1b)
Anchorage, Alaska, USA 244, (15-11)
Andes, South America 202
Anstruther gneiss-dome, Halliburton, Canada 202, (13-23)
Appalachians, Valley-and-Ridge province, USA 103, (7-23)
Arabian Peninsula 66, 212, (5-3), (14-8), (14-9), (17-1)
Arabian plate 66, 154, 157, 158, 210, (5-3), (11-11a & b), (14-8)
Arabian shield, Saudi Arabia 61, 266, (4-16), (16-13, 16-14)
Ardnamurchan, Scotland, UK 199, (13-2), (13-21)
Arecibo deep-space telescope, Puerto Rico 251, (15-20b)
Armero, Colombia 225
Arran, Scotland, UK (13-2)
Aspronsi, Crete, Greece (14-29b & c)
Atlantic plate 227, (14-24b)
Atlantis 231
Australian plate (11-10)
Bald Rock pluton, Sierra Nevada, California, USA (13-22)
Baltic shield, Sweden (1-9b)
Bank Island, North-West Territory, Canada (13-11a)
Bear Butte, Black Hills, South Dakota, USA (7-20)
Bell Fourche River, Black Hills, South Dakota, USA (7-20)

Bikita dome, Zimbabwe, Africa (13-24)
Billefjorden trough, Svalbard, Barents Sea 134, (9-16)
Bingham Canyon Copper Mine, Salt Lake City, USA 6, (1-2a)
Bitlis Suture, Middle East (14-8)
Black Hills, South Dakota, USA 101, (7-20)
Blinman Copper Mine, Australia (10-16)
British coal measures, UK 125, (9-5), (9-8), (12-13)
British Isles, UK 188, (13-2)
Bucks Lake pluton, Sierra Nevada, California, USA (13-22)
Burgess Shale, Grand Canyon, USA 32
Burleigh granite gneiss, Halliburton, Canada (13-23)
Calaveres Fault, California, USA (1-5b)
Camel Peak fault, Sierra Nevada, California, USA (13-22)
Camiguin Island, Philippines 228, (14-26)
Cappodocia, Turkey 208
Caribbean plate 227, (14-24b)
Carlingford, Scotland, UK (13-2)
Carlsbad Caves, New Mexico, USA 251, (15-21)
Cascade pluton, Sierra Nevada, California, USA (13-22)
Cascade Ranges, Washington, USA (14-21a)
Catania, Sicily, Italy 223, (14-20)
Cayeli ore body, Turkey 292, (17-8)
Centre Lake granite gneiss, Halliburton, Canada (13-23)
Cerro Minuto, Sierra Alhamilla, Spain 248, (15-16a & b), (15-17a & b)
Chaman fault, Iran (11-1b)
Charter dome, Zimbabwe, Africa (13-24)
Cheddar granite gneiss, Halliburton, Canada (13-23)
Cheyenne River, Black Hills, South Dakota, USA (7-20)
Chibi dome, Zimbabwe, Africa (13-24)
Chidlaw vein, Gwynnfynnid Gold Mine, Wales, UK 6, (1-2b)
Chilimanzi dome, Zimbabwe, Africa (13-24)
Chindamora dome, Zimbabwe, Africa (13-24)
City Tunnel, Boston, USA (1-9a)
Clemente-Tomas fault, Gulf of Mexico, USA (4-9a & b)
Coconino Sandstone, Meteor Crater, Arizona, USA (15-5)
Columbia basalts, USA 213, (14-13a)
Columbia River Plateau, Washington, USA (14-13a)
Connecticut, fold structures, USA (10-17)
Corsair fault, Gulf of Mexico (4-9a & b)
Cote Blanche Island salt dome, Louisiana, USA (8-2)
Crater Aristarchus, Moon (15-3b)
Crater Euler, Moon (15-3a)
Crater Lake, Oregon, USA 197, 232, 290, (13-4), (14-21a)
Craters of the Moon National Monument, Idaho, USA 213, (14-12b)
Dakota sandstone hogback, Black Hills, South Dakota, USA (7-20)
Dammam Dome, Arabian Gulf, Saudi Arabia (16-3)
Dammam formation, Saudi Arabia 32
Danakil depression, Africa 212
Dead Sea fault, Middle East 154, 158, 159, (1-11b), (11-9)
Dead Sea, Middle East 158, (11-9)
Deccan Plains, India 213, (14-13b)
Deccan traps, India 213, (14-13b)
Dogwood pluton, Sierra Nevada, California, USA (13-22)
Draa Plateau, Morocco (16-19a & b), (16-20)
Draa Valley, Morocco 274, (16-19a & b), (16-20)
Duff River, UK (9-3)

Easter Island 208
Ekofisk oilfield, North Sea 5, (1-1)
El Capitan, Yosemite National Park, California, USA 290
Electron mudflow, Mount Rainier, USA 224, (14-22b)
Elsimore Fault, California, USA (1-5b)
English basin, UK (3-18)
Etna, Sicily, Italy 223, (14-20)
Eurasian plate 10, 157, 210, (1-6b), (13-4), (14-8)
Feather River ultramafic body, Sierra Nevada, California, USA (13-22)
Fiskefjord region, west Greenland (13-25)
Florida, USA 251, (15-20a)
Fujiyama, Japan 221, (14-19a & b)
Gaaserfjord, eastern Greenland (9-14)
Galapagos, Pacific 218
Garlock Fault, California, USA (1-5b)
Glamorgan granite gneiss, Halliburton, Canada (13-23)
Glas Eilean dike, Ardnamurchan, Scotland, UK (13-21)
Glen Cannich, Scotland, UK, UK (10-18a)
Gondwana 212, (14-7)
Goromonzi dome, Zimbabwe, Africa (13-24)
Gran Saline Mine, Morton Salt Company, Texas, USA (1-3b)
Grand Canyon, Arizona, USA 32, 64, 121, 125, (4-19), (6-1), (9-4a & b), (9-5)
Grand Canyon Series, USA 64, 125, (4-19), (9-4a & b), (9-5)
Great Dyke, Zimbabwe 187, (13-1a & b)
Great Lakes region, North America 255, (15-23)
Great Rift Zone, Idaho, USA 213, (14-12b)
Green Canyon area, Gulf of Mexico 111, (8-5)
Greenland, Caledonian gneiss (7-25b)
Grizzly pluton, Sierra Nevada, California, USA (13-22)
Gros Ventre Lake, Wyoming, USA 11, (1-7a & b)
Gros Ventre River, Wyoming, USA 11, (1-7a & b)
Gros Ventre slide, Wyoming, USA 11, 246, (1-7a & b), (15-14)
Gros Ventre Valley, Wyoming, USA 11, (1-7a & b)
Grosses Bluff, Australia 242
Gulf of Aden, Indian Ocean 154, (1-11b)
Gulf of Aqaba, Red Sea 158
Gulf of Mexico, off-shore Louisiana (10-8)
Gullion, Scotland, UK (13-2)
Gutu dome, Zimbabwe, Africa (13-24)
Gwynnfynnid Gold Mine, Wales, UK 6, (1-2b)
Hainesville salt stock, USA (5-1)
Harney Peak, Black Hills, South Dakota, USA (7-20)
Harrat Kishb, Saudi Arabia 212, (14-8), (14-9), (14-11b)
Hawaii, USA 210, 218, 233, (13-7), (14-16), (14-32)
Hawaiian island chain 192, 218
Hayward Fault, California, USA (1-5b)
Hibok-Hibok, Camiguin Island, Philippines 228, (14-26)
Hilina fault, Hawaii (14-16)
Himalayas 202
Honey Hill fault, Connecticut, USA (10-17)
Hoover Dam, Colorado River, Nevada, USA (1-9c)
Iceland 9, 10, 189, 210, (1-6a & b)
Illinoisian end-moraines, North America 255, (15-23)
India 276, (16-24a & b)
Indian Ocean 154 (1-11a & b)
Indian plate (11-1b)

Indonesian archipelago 192
Italy 210
Japanese archipelago 192
Java, Indonesia 232
Jefferson Island salt dome, Louisiana, USA 7, (1-3a)
Jemez Mountains, New Mexico, USA 234, (14-33)
Kaibab Limestone, Grand Canyon and Meteor Crater, USA 32, (15-5)
Kaibab trail, Grand Canyon Series, USA (9-15)
Kamenis, Crete, Greece 232 , (14-29b & c)
Kapoho Crater, Hawaii (14-17c)
Katmai, Alaska, USA 192, 228, (14-27a, 14-28a)
Katmai-Novarupta, Alaska, USA 208
Kauai, Hawaiian Islands, USA (13-7)
Kealakekuo-Kaholo fault system, Hawaii (14-16)
Keban Dam, eastern Anatolia, Turkey 251, (15-18)
Kenya 210
Kilauea, Hawaii, USA 218, (14-16), (14-17a to c)
Kimberley, South Africa 209, (14-3)
Kodiak, Alaska, USA 208
Kodiang Formation (2-17)
Krafla field, Iceland 189, (13-4)
Krakatao, Indonesia 224, 231, 232, (14-30a & b, 14-31)
Lagunillas River, Colombia 225
Lake Char fault, Connecticut, USA (10-17)
Laki rift/fissure, Iceland 213, (14-11a), (14-12a)
Laramide deformation, USA 101
Lipan Point, Grand Canyon, USA 64, (4-19)
Loch Ba, Mull, Scotland, UK (13-20)
Loch Doon, Scotland, UK 199, (13-18)
Loma Prieta earthquake, California, USA 8, (1-5a)
Lyme dome, Connecticut, USA (10-17)
Macizo de Nevera, Sierra de Albarraccin, Spain 15, (1-11a & b)
Madziwa dome, Zimbabwe, Africa (13-24)
Main Ranges, Cambrian shales, Canada (7-7a)
Makkah-Madinah-Nafud volcanic line, Saudi Arabia 212, (14-9)
Makran Ranges, Iran (11-1b)
Mambajao, Camiguin Island, Philippines 228, (14-26)
Mammoth Cave area, Kentucky, USA 251
Manato area, Puerto Rico 251, (15-20b)
Manicouagan ring, Quebec, Canada 242, (15-6b)
Manuapo Kaoiki fault system, Hawaii (14-16)
Manyika dome, Zimbabwe, Africa (13-24)
Mare Imbrium, Moon (15-3a)
Marina district, San Francisco, California, USA 8, (1-5a)
Mars 237, 290, 295
Martinique 227, 228, (14-24a & b)
Matopo dome, Zimbabwe, Africa (13-24)
Maui, Hawaiian Islands, USA (13-7)
Mauna Kea, Hawaii, USA (14-16)
Mauna Loa, Hawaii, USA 218, 233, (14-16), (14-32)
Mazama, Crater Lake, Oregon, USA 197
Meeteetse area, Wyoming, USA 128, (9-9)
Melones pluton, Sierra Nevada, California, USA (13-22)
Menan Buttes, Idaho, USA 263, (16-5)
Mercury 237
Merrimac pluton, Sierra Nevada, California, USA (13-22)

Meteor Crater, Winslow, Arizona, USA 13, 240, 242, (15-5), (1-8b)
Michigan Basin, North America 60, 66, (4-15), (5-2)
Mid-Atlantic rift zone 210
Mid-Atlantic spreading ridge 189
Midway Islands, Pacific (13-7)
Milton area, Greensboro, North Carolina, USA (10-18b)
Minoan civilization, Greece 231, 232
Moenkopi Formation, Meteor Crater, Arizona, USA (15-5)
Moere platform, North Sea, Europe (9-18)
Mojave desert, California, USA 266, (1-5b), (16-11)
Mokuaweoweo collapse pit, Hawaii, USA 233, (14-17a & b), (14-32)
Molakai, Hawaiian Islands, USA (13-7)
Moon 237, (15-3a & b)
Moroccan Border fault, Morocco 275, (16-19a & b), (16-20)
Mount Etna, Sicily, Italy 223, (14-20)
Mount Fuji, Japan 221, (14-19a & b)
Mount Katmai, Alaska, USA 192, 228, (14-27a, 14-28a)
Mount Mazama, Crater Lake, Oregon, USA 197
Mount Pelée, Martinique 221, 224, 226, 227, (14-24a, 14-25)
Mount Rainier, USA 224, (14-22a & b), (14-21a)
Mount Somma, Vesuvius, Italy (14-23a)
Mount St. Helens, Washington, USA 223, 224, 228, 231, 290, (10-10), (14-21a to d), (17-4)
Mount Toc, Italy 246, (15-13a & b)
Mount Vesuvius, Italy 224, 226, (14-23a to d)
Mourne, Scotland, UK (13-2)
Mtoko dome, Zimbabwe, Africa (13-24)
Mull, Scotland, UK 199, (13-2), 13-20)
Muow Limestone, Grand Canyon, USA 121
Nacimiento Fault, California, USA (1-5b)
Navajo Sandstone, Grand Canyon, USA 32
Netherlands, sea dikes, Europe 208
Nevado del Ruiz, Colombia 224, 225
Nevados Huascaran, Peruvian Andes 243, (15-9)
New Zealand 158, 159, 210
North-American plate 10, 210, (1-6b), (11-10), (13-4)
Novarupta, Alaska, USA 228, (14-28b)
Oahu, Hawaiian Islands, USA (13-7)
Old Bierer Cabin, Gros Ventre Valley, Wyoming, USA 17, (1-7b)
Old Faithful, Yellowstone National Park, Wyoming, USA 210
Oliver Lake pluton, Sierra Nevada, California, USA (13-22)
Olympus Mons, Mars 290
Oman ophiolites 188
Osceola mudflow, Mount Rainier, USA 224, (14-22b)
Owen fracture zone, Indian Ocean 154, 158, (1-11b)
Pacific Ocean 192
Pacific plate 192, 218, 221, (11-10), (13-7), (14-19b)
Pacific ridge (14-1)
Pahsimeroi River, South Idaho, USA (15-15)
Palmyra fold belt, Middle East (14-8)
Palomares shear zone, Spain 186, (12-23)
Pangea 210
Paredon basin, Mexico (2-12)
Pelée, Martinique 221, 224, 226, 227, (14-24a, 14-25)
Peru 199, (13-19)
Pilbara block, northwest Australia 206, (13-27)

Point Fermin, California, USA 246, (15-12)
Pompei, Italy 226, (14-23b to d)
Pyrenees, Europe 202
Rainier, USA 224, (14-22a & b), (14-21a)
Ranrahirca, Peru 244
Red Sea 154, 210, 212, (1-11a & b), (14-8)
Red Sea rift zone (11-1a & b), (14-9)
Red Valley, Black Hills, South Dakota, USA (7-20)
Redondo peak, Jemez Mountains, New Mexico, USA 234, (14-33)
Rhodesdale dome, Zimbabwe, Africa (13-24)
Rich Bar pluton, Sierra Nevada, California, USA (13-22)
Richat dome, Mauritania (2-10)
Royal Observatory Greenwich, UK 22
Rum, Scotland, UK (13-2)
Rus formation, Saudi Arabia 32
Rye, New Hampshire, USA (13-10)
Sahba fault, Saudi Arabia 282, (16-27a & b), (16-28)
Saltfjord, Paleozoic schist, Norway (7-7b)
San Andreas fault, California, USA 8, 159, (1-5b)
San Andreas Fault, California, USA (1-5b)
San Gabriel Fault, California, USA (1-5b)
San Jacinto Fault, California, USA (1-5b)
Santa Ynez Fault, California, USA (1-5b)
Santorini, Aegean Sea, Greece 231, (14-29a to c)
Saudi Arabia 212, (14-8), (14-9)
Selden neck, Connecticut, USA (10-17)
Sesombi dome, Zimbabwe, Africa (13-24)
Shangai dome, Zimbabwe, Africa (13-24)
Sheep Mountain, Wyoming, USA 99, (7-17)
Sherman Glacier, Alaska, USA 244, (15-10)
Shinumo Creek, Grand Canyon Series, USA 125, (9-4a & b)
Shiprock Mountain, New Mexico, USA 235, (14-34c)
Sidi Ifni, Morocco 274, (16-19b)
Sierra Alhamilla, Spain 248, (15-16a & b), (15-17a & b)
Sierra de Albarraccin, Spain 15, (1-11a & b)
Sierra Nevada batholith, California, USA 202, (1-5b), (13-6), (13-22)
Siljan ring, Sweden 242, 243, (15-7a & b)
Skalbreidur, Iceland 218
Skye, Scotland, UK (13-2)
Slieve, Scotland, UK (13-2
Snake River Plain, USA 213, (14-12b)
Somma, Vesuvius, Italy (14-23a)
Springerville Volcanic Field, Arizona, USA 294, (17-12)
St. Helens, Washington, USA 223, 224, 228, 231, 290,
(10-10), (14-21a to d), (17-4)
St. Pierre, Martinique 227, 228, (14-24a, 14-25)
Statfjord area, North Sea, Europe 136, (9-18)
Sudbury ring, Canada 242
Suez Canal, Egypt 232
Sumatra, Indonesia 232
Sunda Straits, Indonesia 232, (14-31)
Surtsey, Vestmann Islands, Iceland 9, 210, (1-6a), (14-6)
Svalbard, Barents Sea 134, (9-16)
Tambora, Indonesia 224,
Temple Butte Limestone, Grand Canyon, USA 121
Texas, USA 251

Thera, Crete, Greece 232, (14-29b & c)
Theresia, Crete, Greece (14-29b)
Tigris foredeep, Iran (11-1b)
Tindouf basin, Morocco 275, (16-19a & b),(16-20)
Toc, Italy 246, (15-13a & b)
Tonga Trench, Pacific (11-10)
Tovqussap dome, west Greenland 203, (13-26a & b)
Truchas shear zone, Macizo de Nevera, Sierra de Albarraccin, Spain 17, (1-11b)
Turnagain Heights, Anchorage, Alaska, USA 244, (15-11)
Turrillas, Sierra Alhamilla, Spain 248, (15-16a & b), (15-17a & b)
Umanak area, Precambrian gneiss, Greenland (7-25a)
Vaiont Dam, Italy 246, (15-13a & b)
Vaiont Valley, Italy 246, (15-13a & b)
Valdez, Alaska, USA 244
Valles Caldera, Jemez Mountains, New Mexico, USA 234, 236, (14-33)
Valles Marineris, Mars 295
Valley of Ten-Thousand Smokes, Alaska, USA 228, (14-27b, 14-28a)
Valley-and-Ridge province, USA 103, (7-23)
Venus, Magellan radar image 283, (16-29)
Vestmann Islands, Iceland 9, 210, (1-6a), (14-6)
Vestmann Islands, Iceland 210
Vesuvius, Italy 224, 226, (14-23a to d)
Victoria Land, Antarctica (13-11b)
Vishnu schist, Grand Canyon, USA (9-15)
Vredefort astrobleme, South Africa 242, (15-6a)
Wadi Sahba, Saudi Arabia 282, (16-27a & b), (16-28)
Waiohinu fault, Hawaii (14-16)
Wanda Fault Zone, Gulf of Mexico (4-9a)
Waterpocket monocline, Utah, USA 104, (7-26b)
Wells Creek, Tennessee, USA 242, (15-6c)
Willimanitic dome, Connecticut, USA (10-17)
Winter Park sinkhole, Florida, USA 13, (1-8a)
Wisconsinian end-moraines, North America 255, (15-23)
Wizard Island, Crater Lake, Oregon, USA 197, 232, (13-14)
Wyoming, folded strata, USA 266, (16-12)
Yellowstone National Park, Wyoming, USA 210
Yemen, Middle East (16-15)
Yosemite National Park, California, USA 290, (13-6)
Yungay, Peru 243, 244, (15-9)
Zagros fault, Iran (11-1b)
Zagros Mountains, Iran 61, 101, 102, 154, 157, (4-16), (7-21), (11-1b)
Zagros Suture, Iran (14-8)
Zimbabwe craton, Africa 203, (13-24)
Zwimba dome, Zimbabwe, Africa (13-24)

Subject Index

Acid lava 222
Active continental margin 187, 202
Active remote sensing system 258
Aerial photograph 20, 82, 259, 262-264, 266, 274
Aerial photography 259, 260, 264
Aerial survey 259
Agglutinate 212
Airborne lava fragments 212
Albedo 264
Alkali basalt 212
Alkali magma series 212
Amplitude 89
Ancient shoreline 134
Andesite 222
Andesite dome 226
Andesitic volcanism 192
Angle of dip 39
Angular perspective 138, 140
Angular unconformity 121, 125, 126, 130, 132
Annular depression 243
Annular graben 238
Annular ring-dike 283
Anomalies of pressure 187
Anticline 95, 98, 186
Antiform 94, 98, 173, 174
Apollo 271
Apophyses 194
Apparent dip 40, 41, 48, 51, 55, 61, 62, 64
Apparent thickness 44, 49, 61, 62, 63, 96
Apparent thickness change 59
Appollo flight 240
Arachnoid 283
Archipelago 192
Area coverage 259
Ash 210, 228
Ashfall 207, 224, 226, 228
Ashflow 208
Asthenosphere 158
Astrobleme 237, 241, 242
Asymmetric fold 96
Aulacogen 212
AutoCAD 287, 292
Axial culmination 101
Axial plane 95, 112, 182
Axial plane trace 96, 111, 112
Axial surface 94, 117
Axial trace 94, 95, 98
Azimuth 35, 37
Azimuth/dip 38, 68, 79, 85
Azimuth line 37
Backfolding 238, 241
Backscatter 279
Barchan dune 266
Basalt 208, 212, 213
Basalt flow 188, 210, 212
Basalt lava 212, 213, 218
Base map 260
Basement 66, 132, 158, 266
Basement-uplift 101
Basic dike 212, 266
Basic lava 222
Bathing stone 208
Batholith 190, 199, 202
Batholith complex 190
Black smoker 208
Block and ash deposit 226
Block diagram 30, 49, 96, 132, 143, 144, 163, 194, 203, 214
Blow-out 209
Boomerang-shaped outlier 119
Breached crater 223
Brittle-ductile shear zone 186

Building site 243
Butte 21, 236
Cabinet diagram 151
Caldera 197, 231, 234
Caldera collapse 231, 234
Caldera floor 234
Caldera formation 228
Caldera subsidence 232
Cap rock 109, 134
Casualties 223, 224
Cauldron subsidence 197
Central depression 238
Central fault 186
Central graben 158, 188
Central mound 238, 240
Central rift zone 189
Central stock 235
Central uplift 242
Charge-coupled device 274
Chevron fold 90, 111
Cinder cone 197, 212-214
Clockwise 158
Collapse pit 233
Collision suture 188
Collision zone 154, 190
Columnar section 32
Complex deformation pattern 107
Complex map pattern 132, 168
Composite cone 221
Compositional layering 203
Compositional zonation 199
Computer applications 285
Computer technology 259
Concave slope 221
Concentric fold 92
Concordant relationship 194, 202
Cone 212, 213
Cone sheet 197, 199, 283
Conical fold 94
Conical pipe 209
Constant thickness 59
Contact metamorphism 199
Continental crust 154, 187-189, 192, 210, 212
Continental erosion rate 238
Continental fragment 210
Continental margin 188, 192, 236
Continental rifting 212
Continental separation 212
Contour interval 20
Contour lines 19, 20, 68
Contour map 109, 289
Contour spacing 66
Contrast stretching 276
Convex shape 221
Cooling magma 199
Core-mantle boundary 192
Coulisse diagram 149, 151
Counterclockwise 158
Cover sequence 158, 132
Crater 228, 231, 237, 238, 243
Crater lake 207, 224
Crater rim 238, 241, 243
Craton 188, 203
Crests of fold closures 101
Cross-cutting structures 55
Cross-section 30, 31, 32, 40, 41, 46, 49, 51, 53, 54, 61, 62, 64, 71, 119, 134, 139, 143, 209, 238
Crustal cut-out 138
Crustal extension 154
Crustal shortening 157
Crustal thickening 159
Crustal transfer 158
Cumulus layer 188
Cupola 197
Cylindrical fold 92
D''-layer 192
Data collection 259
Debris-flow 243, 244
Debris-laden mudflow 223
Debris-laden water 225
Deformation patterns 3
Dendritic canyon system 26
Dendritic outcrop pattern 122
Depocenter 59
Depression 209
Dextral 158
Diabase dike 194
Diamond 208, 209
Diamond pipe 209
Diatreme 209
Dielectric constant 281
Diffuse shear 187
Digital elevation model 289, 293
Digital line graph 295
Digital map 287-289
Digital number 275
Digital terrain model 293
Dike 188, 196, 197, 212, 235
Dike swarm 188
Dip 35, 37, 39, 50, 54, 55, 63, 65, 68, 79, 85, 91, 95, 126, 264
Dip exaggeration 55, 56
Dip of the fold limbs 117
Dip separation 160
Dip-slip 169, 183
Dip-slip fault 155, 158, 160, 163, 171, 173, 181, 182
Dip-slope 246, 264
Direction of dip 50
Disconformable layer 122
Disconformable stream channel 122
Disconformity 121, 122
Discontinuous layer 122
Discordant relationship 132, 190, 194
Disharmonic fold 92
Displacement vector 155
Distortional effect 61
Dome 226, 228
Dome emplacement 202
Dome surface 109
Domes and basins 203

Dormant volcano 224
Double tilting 126
Double-vanishing-point perspective 140
Doubly plunging fold 101, 157
Doubly plunging synform 181
Downthrown block 161, 168, 173, 178
Downthrown wall 174
Drainage network 264
Drainage pattern 264, 266
Drift map 249
Drumlin 254
Ductile creep 243
Ductile deformation 184
Dune sand 282
Dynamic digital map 294
Dynamic map 295
Earthquake 213, 223, 243, 244, 246
Effect of topography 144
Ejecta 226
Elastic recovery 238
Electromagnetic energy 258
Electromagnetic radiation 257, 259, 270
Electromagnetic sensor 259
Electromagnetic spectrum 257, 258, 273, 276
Elevated structure-contour diagram 149
Elevation contour 19, 68
Elevation contour map 22
Elongated dome 101, 109
Emplacement 189, 199
Emplacement mechanism 190
En-echelon fracture 212
En-echelon network 101
En-echelon pattern 98, 214
End-moraine 253
Endogenic deformation structure 237
Endogenic processes 237
Energy resource 208
Epiclastic deposits 222
Episodic eruption 218, 223
Episodic pulses 192
Eroded extrusive 235
Erosional disconformity 122
ERTS 273
Eruption 223-225, 228
Eruption center 190
Eruption cone 221
Eruption cycle 218
Eruption source 228
Esker 254
Exaggerated cross-section 59
Exaggerated dip 55, 59
Exaggerated thickness 58
Exaggeration factor 55
Excavation work 226
Exogenic processes 237
Exogenic structure 237
Experimental ground blast 240
Exploitation of volcanic rock 207
Exploration 4
Explosive eruption 221, 222, 228, 231, 232
Exposure width 173
Extensional thinning 187
Extrusion 212
Extrusive igneous rock 208
Facies change 122, 134, 151
Failed rifting 188
Failure surface 246
False color 259, 276
Famine 207, 224
Fault 153, 154
Fault breccia 168
Fault off-set 266
Fault plane 58
Fault separation 160
Fault slip 160, 183
Fault trace 174
Faulted antiform 173
Faulted fold 182-184
Faulted synform 173
Feeder dike 266
Feeder fissure 213
Feeder pipe 235
Felsic tuff 226
Fence diagram 151
Fenster 158
Fiducial mark 262, 266
Fishnet mesh grid 290
Fissure 188, 208, 209, 212
Fissure eruption 212
Fissure system 212
Fissure zone 212
Flat-iron 264
Flight altitude 260
Flight line 263
Flight-path 262
Flood basalt 212-214, 266
Flood warning system 225
Flood wave 207, 224, 232
Fold 89
Fold axis 94
Fold belt 95, 190, 202
Fold closure 98, 114, 171, 173, 178
Fold core 95
Fold crest 91
Fold hinge 91, 101, 178, 181, 182
Fold hinge line 94, 183
Fold limb 53, 89, 91, 112, 117, 182, 183
Fold pattern 173
Fold profile 89, 91, 119
Fold shape 92
Fold through 91
Fold train 89, 91
Fold trend 202
Foliation 202
Foot wall 155, 157, 158
Foreshortening 141
Form line 109, 111, 203
Form-line contour 109, 111
Formation 32
Fractionated mantle rock 154
Fracture 208
Fracture pattern 238

Fracture systems 8
Fracture zone 187, 221, 243
Free-fall velocities 240
Frequency bands 258
Frictional resistance 223
Funnel shape 209
Gas content 222
Gemini 271
Geographic information systems (GIS) 292
Geographical coordinates 144
Geological map 3, 14, 50, 51, 64, 82, 107, 114, 168, 187
Geological setting 187
Geological structure 53
Geological symbol 168
Geomorphology 264, 265
Geoshare 296
Geostatistics 296
Geothermal energy 9, 209, 210
Geyser 210
Glacial 253
Glacial Structure 253
Glaciation 253
Glacier 224, 253
Global positioning system (GPS) 293
Global sea-level drop 126
Globule 228
Glowing avalanche 224, 226, 228, 229
Gneiss-dome 203
Gneissosity 203
Gold 208
Graben 156, 158, 188, 238
Granitic composition 199
Granitic intrusion 190, 192, 266
Gravitational accretion 237
Gravitational collapse 237
Greenhouse 210
Greenstone 203
Ground-moraine 253, 254
Ground motion 243
Ground Penetrating Radar (GPR) 279
Ground penetration 279
Ground resolution 271
Ground separation 260
Ground speed 271
Groundtrack 273
Groundwater reservoirs 8
Group 32
Hachures 21, 168
Half-arrows 168
Hammer-Aitoff projection 210
Hanging wall 154, 155, 157, 158, 161
Hardware 287
Harmonic fold 92
Hazard 8, 207, 224, 225
Hazard map 225
Herring-bone pattern of structure contours 112, 114
Hiatus 121
High-pressure mineral 241
Hinge line 90, 111, 112, 119
Hinge point 89, 90, 91
Hinge zone 91, 112
Homoclinal 30, 75
Horizontal fold 89, 96, 171, 183
Horizontal fold axes 117
Horizontal scale 51
Hornfels 199
Horst 156
Hot gas 226
Hot-spot 192, 218
Hot-spot magmatism 192
Hot spring 234
Hunting tools 208
Hydrocarbon basin 135
Hydrocarbon reservoir 109
Hydrocarbon trap 134, 153
Hydrothermal deposit 208
Ice age 253
Ice cover 223
Ice sheet 207, 253
Igneous complex 199
Igneous dike 187
Igneous extrusive 235
Igneous intrusion 187, 194, 199
Igneous rock 210
Igneous sheet 197
Igneous terrain 187
Ignimbrite 226, 228
Image enhancement 276
Image processing 259, 275
Impact breccia 242
Impact crater 238, 240-242
Impact melt 241
Impact speed 240
Impact structure 237
Impact velocity 241
Imperveous schist 251
Incipient failure 187
Incipient rifting 212
Inclined fold 96, 182
Inclined horizontal fold 111
Inclusions 132
Incomplete map pattern 79
Increased vertical scale 54
Inflection point 90, 91
Infrared band 259, 276
Inlier 79, 80, 158
Insertion of outcrops 82
Interfacing platform 296
Interglacial period 130
Interleafing 222
Interlimb angle 91, 94
Internal slump terrace 240
International date line 22
Internet 287, 288, 295
Intrusive bodies 265
Intrusive igneous rock 199
Inverted relief 234, 236
Island arc 192
Island subsidence 231
Isochore 134, 135
Isometric block 143, 144

Isometric block diagram 141, 144, 145, 290
Isometric map 145
Isometric perspective 141, 144
Isometric projection 144, 149
Isopach 134, 135
Isopach map 134, 135, 228
Juxtaposed plates 158
Kame 254
Karst 251, 253, 282
Kettle 253, 254
Kettle lake 254
Kimberlite 209
Klippe 158
Laccolith 196, 197
Lahar 224
Landsat 259, 271-273, 276, 282
Landsat thematic mapper 271
Landslide 231, 243, 246
Landsliding 243, 244
Large Format Camera 259
Lateral changes in thickness 59
Latitude 22
Lava 210, 222, 223, 228
Lava bomb 226
Lava field 212
Lava flood 213
Lava flow 213, 222-224, 226
Lava sheet 235
Layer thickness 55
Left-lateral 158
Legend 53
Length/thickness ratio 58
Limb curvature 111
Line of section 50, 51
Line scanning 271
Linear fissure 218
Liquefied 244
Lithological symbol 32
Lithospheric plate 153
Locating hydrocarbon accumulations 109
Location map 229
Longitude 22
Longitudinal fault 163, 171, 174, 181
Lost empire 231
Low altitude photograph 259
Low angle fault 157
Lunar craters 240
Maar 209
Magellan 283
Magma 223
Magma batches 199
Magma chamber 194, 199, 208, 232
Magma pipe 209
Magmatic activity 132, 192
Magmatic belt 202
Magmatic emplacement 192
Magmatic episode 199
Magmatic fractionation 199
Magmatic injection 196
Magmatic intrusion 194
Magmatic site 187
Magmatic texture 203
Magmatism 187
Mantle magma 192
Mantled gneiss-dome 202, 203
Map pattern 96, 117, 163, 171, 223
Map symbol 39, 168
Map width 63
Mass wasting 11, 243
Meandering river 264
Melting of ice cap 224
Meltwater 253
Meridian 22
Mesa 21, 236
Metallic sulfide 208
Metamorphic aureole 199
Metasediment 202
Meteorite 240, 241
Meteoritic fragment 238
Meteoritic impact 240
Methane gas 243
Metric Camera 259
Microprocessor 287
Microwave 258
Minimum displacement 158
Minor fold 92
Modulating 275
Monocline 104
Moraine 253
Mountain peak 223
Mountain range 190, 202, 236
Movement trajectory 249
Mud-fraction 253
Mudflow 207, 224-226, 228, 229
Multispectral scanner 271
Namakier 149
NASA missions 271
Natural hazards 8
Neck 196, 209
Nested plutons 202
Net separation 160
Nimbus 271
Non-cylindrical fold 94
Nonconformity 121, 132
Normal fault 154, 155, 163, 168, 181
Normal thickness 44
Normalized exaggerated thickness 58, 59
Nuée ardente 226-228
Obducted 188
Oblique aerial photograph 264
Oblique cross-section 62, 64
Oblique fault slip 183
Oblique profile 41
Oblique section 48, 49, 62
Oblique slip 183
Oblique-slip fault 183
Ocean floor 188, 210, 212, 218
Oceanic crust 188, 189, 212
Oceanic hot spot 218
Oceanic lithosphere 188, 190, 210, 221
Oceanic plate 192
Oceanic spreading pattern 210

Off-lap 126
On-line resources 295
One-point perspective 138
Onlap 126
Onlier 80
Ophiolite 188
Ore body 151
Organic carbondioxide 251
Original layer dip 58
Orogen 202
Orogenic episode 202
Orthogonal thickness exaggeration 58
Outcrop pattern 22, 35, 68, 69, 72, 73, 79, 80, 82, 86, 98, 114, 117, 181
Outcrop pattern of folded strata 114
Outcrop width 96
Outlier 79, 80, 158
Outwash plain 253, 254
Overlap 126
Oversteepening 246
Overstep 126
Overturned fold 91, 96
Overturned horizontal fold 96
Panchromatic image 274, 275
Parallel drainage pattern 264
Parallel perspective 137, 138
Parallel sections 151
Partial melt 212, 190
Passive imaging system 258
Pegmatite vein 208
Penetration depth 282
Peripheral depression 242
Perspective diagram 137-141
Petroleum exploration 271
Petroleum industry 297
Photo interpretation 263, 264
Photo interpretation-map 260, 266
Photo-mosaic 262
Photogeological interpretation 263-265
Photogeology 263
Photographic band 258
Pit 233
Pixel 272, 275, 276, 280, 287
Pixel resolution 274
Pixel size 273
Pixel tone 275
Planetary interior 243
Plate boundary 154, 187, 192, 212
Plate tectonic evolution 210
Plate tectonics 210
Plug 209
Plunge 37, 98, 112
Plunge line 37
Plunging antiform 96
Plunging chevron fold 112
Plunging fold 44, 62, 96, 98, 112, 132, 177, 181
Plunging synform 178
Pluton 190, 197, 203, 266
Plutonic mass 190
Pore pressure 223
Pore water pressure 246
Pressure wave 228
Principal point 262
Print laydown 262
Processing speed 287
Profile line 48, 62
Protoplanets 237
Protractor 144
Pseudotachylite 241
Pumice 208, 226
Pumiceous ash 228
Pyroclastic deposits 208, 209, 222, 223, 226
Pyroclastic flow 223, 228
Pyroclastic material 218
Pyroclasts 212
Quantitative Structural Mapping 270
Radar band 258
Radar image 279, 282
Radar microwave 282
Radar pulse 280
Radial dike 197
Radial distortion 270
Radial ejecta 238
Radial fissure 223
Radial igneous dike 283
Radial ridge 235
Rarefaction 238
Reclined fold 104
Recumbent fold 104
Reflective infrared spectral band 258
Regional survey 262
Regional trend 49
Regression 126
Relative age 95
Relative displacement 160
Relative thickness 32
Remote sensing 257
Reservoir 134, 135
Reservoir model 296
Resolution 260, 271, 272
Reverse fault 155, 157, 160, 168, 173, 174, 178
Rhyolite 241
Rhyolite dome 234
Rhyolite flow 234
Ridge axis 208
Rift 210, 212, 213
Rift arm 212
Rift valley 154, 212
Rift zone 187, 189, 210, 212, 214, 218
Rifting 154, 189, 210
Right-lateral 158
Ring dike 197, 199
Ring structure 242
Rock avalanche 243, 244
Rock fragment 226
Rock mechanics 16
Rock slide 232, 249
Roof pendant 197
Run, flight path 262
Salt body 66, 149
Salt dome 54, 109, 149

Salt glacier 149
Salt mass 143
Salt stock 101
Satellite image 101, 242, 260, 270
Satellites 271
Scale exaggeration 62
Scale model 151
Scale of resolution 259
Scaling of sections 54
Scan line 272
Scoria cone 213
Scoriaceous pyro-clastics 212
Sea dike 208
Sea-level datum 88
Seal rock 109
Seasat 271, 273
Section 50
Section line 30, 40, 62
Seiscrop map 143
Seismic reflection profile 54, 55, 109
Seismic section 59
Seismic tremor 232
Seismogram 57
Sense of movement 158
Sense of shear 168
Serial cut 151
Serial number 262, 266
Shaded relief map 145
Shatter cone 241, 242
Shear fault 158
Shear zone 16, 184, 186
Sheet 188
Shield volcano 218
Shock front 238
Shockwave propagation 241
Sidelap 262
Silica fraction 222
Sill 196, 197
Similar fold 92
Single-vanishing point perspective 138
Sinistral 158
Sinkhole 13, 251
Sinuous ridge 253
Site investigation 5, 13, 14, 246
Slide 223, 243, 246
Slip vector 155
Slope of the terrain 51
Slump mass 243
Smoldering ejecta 226
Snout 244
Software 287, 288
Solar nebula 237
Solar System 237
Solfatare 234
Solidifying melt 187
Solution cavity 251
Space Shuttle 281
Spatter cone 212
Spectral band 258, 259
Splaying 212, 214
SPOT 259, 270, 271, 273, 274
Spreading 189
Spreading ridge 154, 189, 210
Spreading zone 212
Steam 226
Steam eruption 210
Stereo vision 263
Stereopair 263, 266
Stereoscope 263
Stereoscopic view 262
Stock 209
Strain analysis 186
Strain-distance histogram 186
Stratigraphic section 173
Stratigraphic succession 80, 95
Stratigraphic thickness 32, 135
Stratigraphic unit 32, 135
Stratovolcano 21, 221-224, 226, 231
Stream channel 264
Strike 35, 37, 40, 44, 48, 50, 62-64, 65, 68, 79, 109, 126, 158, 163, 171
Strike angle 37
Strike/dip 85, 111
Strike/dip notation 38
Strike/dip symbol 39, 65
Strike line 37, 39, 82, 85
Strike line orientation 39
Strike separation 160, 181-183
Strike-slip 159, 183
Strike-slip fault 158, 168, 182
Strike-slip movement 158, 181
Structural geology 3, 4, 16, 17
Structural high 109
Structural profile 54
Structural section 54
Structural strike 62
Structural symbol 39, 266
Structural trap 89
Structural trend 49
Structure contour 50, 65, 66, 68, 69, 71, 75, 79, 82, 85, 107, 109, 111, 112, 114, 117, 119, 134, 151, 168, 183
Structure-contour map 5, 65, 66, 68, 73, 107, 109, 111, 112
Subduction 190
Subduction island arc 187, 192
Subduction zone 221, 227, 236
Subglacial tunnel 254
Submarine geyser 208
Submarine mass-displacement 232
Subsidence rate 135
Subsurface data 53
Subsurface structure 41
Subvolcanic complex 197, 199, 283
Suffocation 228
Sulfide deposit 208
Summit collapse 223
Supercontinent 210
Supergroup 32
Superstructure 251
Supracrustal 202, 266
Surface trace 49

Surge 228
Survey map 243
Swarm 188
Swath 271
Syncline 95, 98
Synform 94, 98, 173, 174
Synformal core 171
Syntectonic 202
System resolution 260
Tabular igneous bodies 197
Tabular or sheet like bodies 187
Tearing apart 210
Tectonic map 158
Tectonic plate 154, 190, 210
Tectonic setting 153
Tectonic uplift 126
Tectonics 16
Tephra 226
Terrestrial planets 237
Texture 265
Thematic mapper 272
Thermal band 258
Thermal expansion 197
Thermal infrared band 258
Thickness contour 134
Thickness exaggeration 58
Thickness exaggeration factor 63
Tholeiitic basalt 212
Three-dimensional structure 141
Three-point problem 79, 85, 86, 107
Three-point problems for borehole data 88
Thrust belt 190
Thrust fault 157, 168
Thrust nappe 157
Till 253, 254
Tilted 126
Time-averaged rate 158, 159, 210
Time-averaged spreading rate 189
Time-gap 122, 125
Time span 218
Tiros 271
Tone on aerial photograph 265
Topographic contour 26, 30, 32, 35, 51, 65, 66, 69, 82, 184
Topographic contour map 107, 260
Topographic contourline 82
Topographic elevation 50
Topographic elevation contour 86
Topographic map 19, 20, 22, 145
Topographic relief 72, 114, 132, 184, 282
Topography 168, 228
Trace of the axial plane 96
Transcurrent fault 158
Transfer fault 158
Transform fault 158
Transpression 159
Transtension 159
Transverse fault 163, 171, 173, 178, 182, 243
Trap, volcanic 213
Trend 68, 82, 117
Trough 134
True dip 37, 40, 41, 44, 48, 55, 56, 61, 62, 64
True thickness 44, 48, 49, 50, 55, 63, 134, 135
True-to-scale section 58
Tsunami 207, 233, 244
Two-point perspective 140
Types of folds 92
Unconformity 32, 121, 122, 126, 132, 134
Underground mapping 7
Unequal length scales 54
Uniform dip 86
Uniformly inclined bed 171
Universal resource locator 295
Updoming 197
Uplift 101, 130, 157, 236
Upper plate 168
Upright fold 91, 94
Upright horizontal fold 95, 114, 117
Upright horizontal synform 174
Upright plunging fold 114
Upside-down sequence 95
Upthrown block 161, 173, 178
Upthrown wall 174
Uranium 208
UV-band 259
V-cusps 30
V-pattern 25, 50, 264
V-rule 22
V-shape 22, 30, 264
Vanishing point 139-141
Vent zone 214
Vertical airphoto 266
Vertical exaggeration 30, 51, 54, 56, 58, 143, 263, 264
Vertical exaggeration factor 54, 56, 58, 59
Vertical scale 48, 55
Vertical sheet 151
Vertical thickness 63, 134
Vertically exaggerated section 54
Violent eruption 223, 224, 232
Visible light 259
Visual distortion 62
Volcanic activity 224, 234, 283
Volcanic archipelago 231
Volcanic ash 226
Volcanic belt 192
Volcanic cone 196
Volcanic ejecta 228
Volcanic eruption 207, 232
Volcanic gas 223
Volcanic island chain 192
Volcanic landscape 235
Volcanic line 212
Volcanic neck 235
Volcanic outburst 199
Volcanic province 213, 236
Volcanic region 209
Volcanic soil 208
Volcanic structure 236
Volcanic superstructure 232

Volcanic terrain 224
Volcano 192, 197, 223, 229, 263
Volcano summit 223, 225
Volcanogenic structure 207
Volumetric principle 135
Water-content 187
Water reservoir 246
Water-saturated clays 246
Water vapor 228
Wavelength 89
Wavelength bands 258
Welded tuff 234
White smoke 228
Window 158
World Wide Web 295
Wrench fault 158
Zoned plutons 199

Multilingual Abstracts

الجيولوجيا البنيوية وتحليل الخرائط :
د. روود ويجرمارس
قسم علوم الأرض - جامعة الملك فهد للبترول والمعادن
ترجمة : د. عبداللطيف أحمد قحوش

يدرس نظام الجيولوجيا البنيوية معمارية الأرض وبعض الكواكب الأخرى. إن لأنماط تشوه الصخور ملامح مثيرة بسبب جمالها الفنى وأهميتها الإقتصادية للإنسان. إن معرفة البنية التحت سطحية حيوى لنجاح عديد من البرامج الهندسية وبرامج إستكشاف المعادن. إن الفهم الكامل لبنيات الصخور ضرورى للتخطيط فى صناعات البترول والتعدين، وفى عمليات البناء، وفى تصريف النفايات، وفى إستكشاف المياه. لبنيات التشوه فى الصخور أهمية بالغة فى تحديد المناطق الخطرة مثل الكتل الصخرية المحتمل إنهيارها، وفى إنخساف الأرض والفوالق الزلزالية. يتركز نشاط البحوث على بنيات تشوه الصخور فى قشرة القارات القريبة من السطح.

صمم كتاب الجيولوجيا البنيوية وتحليل الخرائط لطلاب البكالوريوس فى الهندسة المدنية، هندسة البترول، تقنية التعدين، علم المياه، دراسات البيئة، والجيوفيزياء، والجيولوجيا. ولقد عرضت مبادئ الجيولوجيا البنيوية بحرص, وتم عرض وشرح المواضيع بنظام متناسق ومدعما بصور توضيحية وتمارين متداخلة فى تفسير الخرائط. وتغطى مادة هذا الكتاب فصل دراسى واحد وتساعد على تحقيق إتصال إنسيابى بين الطلاب ومدرسيهم، وتزودهم بلغة مشتركة فى تقنيات ومبادئ علم الجيولوجيا البنيوية. وبما أن النظرية مدعومة بالتمارين التطبيقية، لذا يمكن إستخدام هذا الكتاب للمحاضرات والمعمل. وإن إستخدام كتاب واحد يشتمل على حزمتين متكاملتين أفضل عمليا من كتابين منفردين، كما أنه يبقى التكلفة الشرائية فى مقدور الطالب.

Структурная геология и интерпретация карт
Автор: Вайермарс, Руд
Аннотацию перевел канд. геол.-мин. наук В.Б.Алексеев
Текст аннотации состоит из двух абзацев

Структурная геология изучает строение твердой Земли и других планет. Деформации горных пород очаровывают и возбуждают фантазию благодаря своей красоте и практическому значению для человека. Знание стуктуры земной коры необходимо для успеха в большом количестве различных программ, связанных с инженерной геологией и полезными ископаемыми. Ясное понимание структуры горных пород важно для стратегического планирования в нефтяной и горной промышленности, строительстве, захоронении отходов и гидрогеологии. Деформационные структуры вмещающих пород влияют на размещение зон повышенной опасности, таких как оползни, области усадки грунта и сейсмичные разломы. Исследования концентрируются на изучении деформационных структур приповерхностной континентальной коры.

Курс "Стуктурная геология и интерпретация карт" разработан для студентов, обучающихся по специальностям гражданское строительство, нефтяная инженерия, технология шахт, гидрология, защита окружающей среды, геофизика и геология. Принципы структурной геологии тщательно изложены и разработаны систематически. Они сопровождаются иллюстрациями и упражнениями по интепретации карт. Эта сводка охватывает один семестр лекций и помогает установить легкий контакт между преподавателями и студентами, обеспечивая общий язык по методам и принципам структурной геологии. Поскольку в этой книге теория совмещена с упражнениями, она может использоваться как для лекций, так и для практических занятий. Использование единой книги, освещающей два взаимосвязанных аспекта—теоретический и практический,— вместо двух отдельных книг, практично и позволяет сделать ее цену доступной для студентов.

構造地質學與地圖解釋 (Structural Geology and Map Interpretation)
儒德 魏捷馬斯 著
盧佳遇 譯

構造地質學的訓練是用來研究地球與其他行星的架構。岩石的變形圖案是令人興奮的現象，因爲它們不但具有美感同時兼具經濟價值。認識地下構造是各類工程與礦物探勘計劃成功的必要條件。對岩石構造的徹底瞭解亦是石油與礦冶工業，大型建築，廢料處理及水源探勘所不可或缺的。圍岩的變形構造對於潛在的岩石滑動，地層下陷，地震斷層等的定位非常重要。構造地質學的研究集中在大陸地殼淺部的岩石變形構造。

〞構造地質學與地圖解釋〞一書是針對大學部，主修土木工程，礦冶技術，水文學，環境科學，地球物理與地質學等的學生所設計。文中謹愼的介紹構造地質學原理與系統性的發展，伴隨著說明圖表與深入淺出的地圖解釋習題。這本運用已知最新知識、技術的教課書，可以涵蓋一學期的課程，並且可以建立學生與教師間簡化而有效率的溝通，同時提供了構造地質學原理與方法上的共通語言。因爲理論與實習的結合，這本書可同時在講堂與實驗室中使用。因此本書也較一般分爲兩冊的教課書更爲實用且價錢合宜學生購買。

Geología Estructural e Interpretación de Mapas
(Structural Geology and Map Interpretation)
Autor: Ruud Weijermars
Traducido por: Julia Cuevas

A manera de introducción

La disciplina de la *geología estructural* estudia la arquitectura de la Tierra sólida y de otros planetas. Los modelos de deformación de las rocas son rasgos apasionantes debido a su belleza estética y a su interés económico para el hombre. El conocimiento de las estructuras del subsuelo es vital para el éxito de muchos programas de exploración minera y de ingeniería. La comprensión minuciosa de las estructuras de las rocas es esencial para una planificación estratégica en la industria minera y del petróleo, en la construcción, en estudios para la ubicación de vertederos y para la prospección de aguas subterráneas. Las estructuras de deformación en la roca encajante son además importantes para la localización de zonas de riesgo, tales como potenciales zonas de deslizamientos de ladera, hundimiento del suelo y fallas sísmicas. Las actividades de investigación se concentran en las estructuras de deformación de las rocas de la corteza continental superficial.

Este libro, titulado *Geología Estructural e Interpretación de Mapas,* está proyectado para estudiantes de ingeniería civil, ingeniería del petróleo, tecnología minera, hidrología, estudios medioambientales, geofísica y geología. Los principios de geología estructural son introducidos cuidadosamente y desarrollados sistemáticamente, acompañados por ilustraciones informativas y ejercicios perspicaces sobre interpretación de mapas. Esta presentación actualizada cubre un semestre de enseñanza y ayuda a establecer una comunicación más eficiente entre los estudiantes y sus profesores, proporcionando un lenguaje común sobre las técnicas y los principios de la geología estructural. Debido a que la teoría está combinada con ejercicios prácticos, este libro puede usarse tanto para cursos teóricos como para prácticas de laboratorio. El uso de un único libro de texto que integra teoría y problemas es más práctico que dos libros de texto separados y tiene un coste asequible para estudiantes.

Structural Geology an Map Interpretation
Author: Ruud Weijermars
Translated by: Jean Louis Vigneresse

By way of introduction

La discipline de la géologie structurale concerne l'architecture de la Terre et des planètes internes. Les structures des roches déformées sont passionnantes par leur beauté intrinsèque, mais aussi par leur intérèt économique pour l'homme. La connaissance des structures de subsurface est nécessaire à la réalisation et au succès de la planification dans l'industrie minière et pétrolière, lors de la construction d'ouvrages d'art, et à la mise en place de dépôts de déchets ou à la recherche d'eau. Les structures de la déformation des roches sont aussi indispensables pour localiser les zones à risques telles que les glissements de terrain, les affaissements de sols et les failles séismiques. Les activités de recherche se concentrent sur les structures de la déformation des roches dans la croûte continentale superficielle.

L'ouvrage "Structural Geology and Map Interpretation" est destiné aux étudiants de premier cycle en génie civil, génie pétrolier, technologie minière, hydrologie, environnement, géophysique et géologie. Les principes de la géologie structurale sont soigneusement introduits, puis systématiquement dévelopés et accompagnés d'illustrations et d'exercices pertinents sur l'interprétation en carte. Cette somme de connaissances recouvre un semestre d'enseignement et est conçue comme un fil conducteur entre les étudiants et leurs enseignants, sous la forme d'un langage commun sur les techniques et principes de la géologie structurale. Dans la mesure où la théorie est accompagnée d'exercices pratiques, cet ouvrage peut servir à la fois en cours et lors de travaux personnels. L'usage d'un seul manuel comprenant ces deux volets plutôt que deux livres séparés comporte également un coté pratique, et à la fois économique, pour les étudiants.

Structural Geology an Map Interpretation
Author: Ruud Weijermars
Translated by: Stefan Schmid

By way of introduction

Die Disziplin *Strukturgeologie* behandelt die Architektur der festen Erde und anderer Planeten. Muster der Gesteinsdeformation sind faszinierend, sowohl wegen ihrer Aesthetik als auch wegen ihrer ökonomischen Bedeutung für die Menschheit. Kenntnis über den geologischen Untergrund ist entscheidend für den Erfolg einer ganzen Reihe von Massnahmen in Ingeneurgeologie und Lagerstättenkunde. Die strategische Planung der Exploration von Erdöl- und mineralischen Lagerstätten und Wasserresourcen, der Ausführung von Grossbauten als auch von Deponien verlangt ein vertieftes Verständnis der Strukturgeologie. Deformationsstrukturen im Umgebungsgestein sind entscheidend für die Lokalisierung von Gefahrenzonen wie potentielle Bergstürze, Senkungen des Untergrunds oder seismische Aktivität.

Structural Geology and Map Interpretation ist ein Text, welcher sich an Absolventen eines Grundstudiums in Gebieten wie Bauingenieurwesen, Erdölexploration, Lagerstättenkunde, Hydrologie, Umweltwissenschaften, Geophysik oder Geologie richtet. Die Grundlagen der Strukturgeologie werden sorgfältig eingeführt und systematisch weiterentwickelt. Sie sind begleitet von instruktiven Abbildungen und Uebungen in Karteninterpretation. Der aktuelle Text umfasst in etwa den Lehrinhalt eines Semesters und ermöglicht einen geführten Dialog zwischen Studierenden und Dozierenden, indem er eine gemeinsame Terminologie betreffend Techniken und Grundlagen der Strukturgeologie vermittelt. Da der Text mit Uebungen verbunden ist, kann er sowohl für Vorlesungen als auch Praktika benützt werden. Der Gebrauch eines einzigen Lehrbuchs mit integrierten Uebungsblöcken an Stelle von zwei separaten Bänden ist handlich und reduziert die Anschaffungskosten für die Studierenden.

Additional Resources

NEW DIRECTORY OF COMPUTER AND REMOTE-SENSING RESOURCES FOR GEOSCIENCE MAPPING

Directory

Computer and Remote-Sensing Resources for Geoscience Mapping

TECHNOLOGICAL ADVANCES have secured an expanding role for computer and remote-sensing applications in geoscience mapping. This directory includes display advertisements by carefully selected suppliers of products and services related to modern mapping technologies. They offer professional solutions for specific problems that can occur in the interpretation, integration, storage, and retrieval of geological information in surface and subsurface maps. The organizations listed here are involved with one or more of the following technologies: remote-sensing methods, satellite imagery, aerial surveys, digital maps, GIS, GPS, image processing, Multimedia, Hypermedia, computer hardware, software, and interfacing platforms.

AAPG DATA SYSTEMS
P.O. Box 702708
Tulsa, OK 74170
USA
Tel. 918 496-7777
Fax: 918 496-3756
E-mail: rhart@neosof-t.com

ADOBE SYSTEMS INCORPORATED
1585 Charleston Road
Mountain View
CA 94039-7900
USA
Tel. 415 961-4400
Fax: 415 961-3769

ADVANCED LOGIC RESEARCH
9401 Jeronimo
Irvine, CA 92718
USA
Tel. 714 581-6770

AERIAL DATA REDUCTION
9285 Commerce Hwy.
Pennsauken, NJ 08110
USA

AERO SERVICE
8100 Westpark
P.O. Box 1939
Houston, TX 77251
USA

AERO-METRIC ENGINEERING, INC.
4708 North 40th Street
Sheboygan, WI 53083
USA

AERODAT
11999 Katy Fwy
Suite 290
Houston, TX 77079
USA

AEROFILMS, LTD.
Gate Studios
Station Road
Borehamwood
Hertfordshire WD6 1EJ
UK
Tel. 44 81 207 0666
Fax: 44 81 207 5433

AEROMAP U.S., INC.
2014 Merrill
Field Drive
Anchorage,
AK 99501
USA

AEROSUL S/A LEV. ESPACIAIS
Av. Brasilia
5547
Curitiva,
Paran 81020
Brazil

AEROTERRA S.A.
Gorostiaga 2465
Buenos Aires 1426
Argentina

AIR-LAND SURVEYS, INC.
7990 M-15
Clarkston, MI 48348
USA

AIRMAG SURVEYS
P.O. Box 16157
Philadelphia, PA 19114
USA

AIRQUEST RESOURCE SURVEYS, LTD.
15 Trottier Bay
Winnipeg, Manitoba
Canada, R3T 3R3

ALDUS CORP.
411 First Avenue South
Seattle
WA 98104-2871
USA
Tel. 800 333-2538
Fax 206 343-4240

AMERICAN DIGITAL CARTOGRAPHY
3003 West College
Avenue, Appleton
WI 54914
USA

APPLIED GEOPHYSICAL SOFTWARE
P.O. Box 218470
Houston, TX 77218
USA
Tel. 713 578-6000
Fax: 713 784-9917

ARTSCAN DATAMAP
56 Oakmeadow Blvd.
Scarbor
Canada, M1E 4G1

ASC SCIENTIFIC
Corte del Nogal, Suite 1
Carlsbad, CA 92009
USA
Tel. 619 431-2655
Fax: 619 431-0904

AUSTROMAP
Italienerstraße 3
Villach, A-9500
Austria

BARTHOLOMEW
77-85 Fulham Palace
Road, Hammersmith
London W6 8JB
UK

BORLAND INTERNATIONAL, INC.
1800 Green Hills Rd.
Scotts Valley
CA 95067
USA
Tel. 800 331-0877

BUREAU DE RECHERCHES GEOLOGIQUES
Box 6009, Orléans
Cedex 45060
France
Tel. 33 38 64 3434

BUREAU OF ECONOMIC GEOLOGY
University Station
Box X, Austin
TX 78713-8924
USA
Tel. 512 471-7144
Fax: 512 471-0140

CAD IMAGES, INC.
2807 Parham Road
Suite 104
Richmond, VA 23294
USA

CADSCANNING, INC.
2360 W. Commodore
Way, Seattle
WA 98199
USA

CALCOMP
2411 West La Palma
Avenue, Anaheim
CA 92801
USA

CAMBRIAN MAPPING SERVICES, LTD.
Mayfield, Llanbadoc,
Usk, Gwent NP5 1BT
UK
Tel. 44 291 673 022
Fax: 44 291 673 023

CAMBRIDGE PALEOMAP SERVICES
P.O. Box 246
Cambridge CB2 3DW
UK
Tel. 44 223-333 4399
Fax: 44 223-333 4399

CENTRE FOR REMOTE SENSING
2464 Sheffield Road
Ottawa, Ontario
Canada, K1A 0Y7

CART/O/INFO AG
Guetstrasse 10b
CH-8274 Dagerwillen
Switzerland

CARTA CONSULTORIA
Rua Hungria, 574
Sao Paulo
Brazil

CARTO LOGIX CORP.
702-10 Kingsbridge
Garden Circle
Mississauga, Ontario
Canada, L5R 3K6

CARTOTECH, INC.
11900 Crownpoint Dr.,
Suite 100
San Antonio, TX 78233
USA

CD TECHNOLOGY
766 San Alevo Ave.
Sunnyvale, CA 94086
USA

CENTRAL POINT SOFTWARE
15220 NW Greenbrier
Pkwy., Suite 200
Beaverton, OR 97006
USA
Tel. 800 445-4208
503 690-8090
Fax 503 690-8083

CHART INFORMATION SYSTEMS, LTD.
6882 52nd Avenue
Red Deer, Alberta
Canada, T4N 4L1
Tel. 403 347-3733
Fax: 403 347-3150

CIMAGE CORP.
100 Pacifica, Suite 400
Irvine, CA 92718
USA
Tel. 714 753-0272
Fax: 714 753-8879

COGNISEIS DEVELOPMENT
240 Portsmouth Street
Houston, TX 77098
USA
Tel. 713 526-3273
Fax: 713 630-3968

COLOURMAP SCANNING, LTD.
93-99 Upper Richmond
Road
London SW15 2TG
UK

COMPUTER MAPPING COMPANY
3780 Country Road
129 Hesperus
CO 81326
USA

COMPUTER TERRAIN MAPPING, INC.
1401 Walnut, Suite C
P.O. Box 4982
Boulder, CO 80306
USA

CONDOR EARTH TECHNOLOGIES, INC
P.O. Box 3905
Sonora, CA 95370
USA

CONTERRA SYSTEMS
888 43rd Avenue
San Francisco
CA 94121
USA

DATAMAP, INC.
7525 Mitchell Road
Eden Prairie, MN 55344
USA

DATAPLOTTING SERVICES, INC.
200 Cochrane Drive
Unit 4, Markham
Ontario
Canada, L3R 8E8
Tel. 416 513-0036
Fax: 416 513-1425

DEFENSE MAPPING
Aerospace Agency
Center, St. Louis
Missouri
USA

DFVLR
Oberpfaffenhofen
8031 Wessling
Germany

DIGIMAP DATA SERVICES, INC.
37 Kodiak Crescent,
Unit 3, North York
Ontario
Canada, M3J 3E5

DIGITAL IMAGES, INC.
1616 Glenarm Place
Suite 2050, Denver
CO 80202
USA

DIGITAL PETROPHYSICS HOUSTON
2313 W Sam Houston
Pkwy, Suite 145
Houston, TX 77043
USA
Tel. 713 461-6676

DYNAMIC GRAPHICS, INC.
1015 Atlantic Avenue
Alameda, CA 94501
USA
Tel. 510 522-0700
Fax: 510 522-5670

EARTH 'N WARE
4514 Dresden Road
Baltimore, MD 21208
USA
Tel. 410 655-3741
Fax 410 655-3741

EARTH IMAGES
P.O. Box 43, Koynsham
Bristol, BS18 2TH
UK
Tel. 44 275 839 643
Fax: 44 275 839 643

EARTH INFO SCIENCES
241 Warner Road
Lancaster, NY 14086
USA

EARTH OBSERVATION SATELLITE
401 W Main, Suite 390
Norman, OK 73069
USA
Tel. 405 321-4222

EARTH OBSERVATION SATELLITE COMP.
4300 Forbes Blvd
Lanham, MD 20706
USA
Tel. 301 552-0500

EARTH RESOURCE MAPPING
4370 La Jolla Vill. Dr,
Suite 900
San Diego, CA 92122
USA
Tel. 619 558-4709
Fax: 619 558-2657

EARTH SATELLITE CORP.
6011 Executive Blvd.,
Suite 400
Rockville, MD 20852
USA

EARTH SCIENCE SYSTEMS, LTD.
1 Bamfield Court,
Harpenden
Hertfordshire, AL5 5TL
UK
Tel. 44 582 766 288
Fax: 44 582 462 011

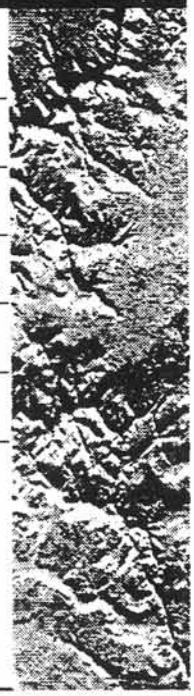

EARTHSAT DATA CENTRE
Edenbridge
Kent, TN8 6HS
UK
Tel. 44 732 865 023

EASTMAN KODAK COMPANY
343 State Street
Rochester, NY 14650-0519
USA
Tel. 716 724-6404
Fax 716 724 9829

ENERGY DATA SERVICES, INC.
1278 FM 407, Suite 109
Lewisville, TX 75067
USA
Tel. 214 317-8446
Fax: 214 317-00085

ENIGMA SOFTWARE, LTD.
750, 840 6th Ave. SW
Calgary, Alberta
Canada, T2P 3E5
Tel. 403 265-2750
Fax: 403 262-1929

FRACTAL DESIGN CORP.
P.O. Box 2380
Aptos, CA 95001
USA
Tel. 408 688-8800

FUJITSU EUROPE, LTD.
2 Longwalk Road
Stockley Park, Uxbridge
Middlesex UB11 1AB,
UK
Tel. 081 573 4444
Fax: 081 573 2643

GAPS GEOLOGICAL CONSULTANTS
13 Deodar Road
Putney, London, SW1 2NP
UK
Tel. 44 81 788 9393
Fax: 44 81 789 9456

GEMINI DRAUGHTING SERVICES
Line House, Barnstone
Nottingham, NO13 9JN
UK
Tel. 44 949 61071
Fax: 44 949 61178

GEO AERIAL
PHOTOGRAPHY
4 Christian Fields
London, SW16 3JZ
UK
Tel. 44 81 764 6292
Fax: 44 81 764 6292

GEO DECISIONS, INC.
301 N. Science Park
Road, State College
PA 16801
USA

GEOAPPLICATIONS
P.O. Box 41082
Tucson, AZ 85717
USA

GEOCART, S.A.
Avda. de America, 49
Madrid, 28002
Spain

GEOCODE, INC.
2612 London Road
Eau Claire, WI 54701
USA

GEOCOMP CORP.
66 Commonwealth
Avenue, Concord
MA 01742
USA
Tel. 508 369-8304
Fax: 508 369-4392

GEOFILMS, LTD.
12 Thame Lane,
Culham, Abingdon
Oxfordshire, OX14 3DS
UK
Tel. 44 235 555 422
Fax: 44 235 530 581

GEOFYZIKA A.S.
Jecna 29a, P.O. Box 62
Brno, 612 46
Czech Republic
Tel. 42 5 776 4111
Fax: 42 5 4122 5089

GEOGRAPHIC DATA
TECHNOLOGY, INC.
11 Lafayette St.
Lebanon, NH 03766
USA

GEOGRAPHIC
SERVICES CORP.
Burton House, 2nd
Floor, Norwich
VT 05055
USA

GEOGRAPHIX
1860 Blake Street,
Suite 900, Denver
CO 80202
USA
Tel. 303 296-0596
Fax: 303 292-1143

GEOLOGIC SYSTEMS,
LTD.
540 5th Ave. SW
Calgary, Alberta
Canada, T2P 0M2
Tel. 403 262-1992

GEOLOGICAL COM-
PUTER SERVICES
1219 E Douglas
Wichita
KS 67211-1605
USA
Tel. 316 264-7807

GEOLOGICAL SURVEY
OF CANADA
601 Booth Street
Ottawa, Ontario
Canada, K1A 0E8
Tel. 613 995-4342
Fax: 613 943-0646

GEOMAP
1100 Geomap Lane
Plano, TX 75074
USA

GEOMATH
200 W Lake Park Blvd.
Suite 1125, Houston
TX 77079
USA

GEOPHYSICAL
SURVEY SYSTEMS
P.O. Box 97
North Salem
NH 03073-0097
USA

GEOPLANE SERVICES
CORP.
1811 Bering Drive,
Suite 277, Houston
TX 77057
USA

GEOSOFT EUROPE,
LTD.
16A Whilchurch Road,
Pangboume
Reading, RG8 7BP
UK
Tel. 44 734 841 280
Fax: 44 734 841 278

GEOSOLVE
19 Rodenhurst Road
London, SW4 8AE
UK
Tel. 44 81 674 7251
Fax: 44 81 674 9685

GEOTECH COMPUTER
SYSTEMS, INC.
7338 S Alton Way,
Suite 16F, Englewood
CO 80112
USA
Tel. 303 740-9432
Fax: 303 740-9542

GIS CONSULTANTS
1615 Broadway
Suite 415
Oakland, CA 94611
USA

GISNET BBS
1401 Walnut Street,
Suite C, Boulder
CO 80302
USA

GLOBAL EARTH
SCIENCES SERVICES
No. 2 Flight Hangar,
Leavesden, Airport,
Watford
WD2 7BZ, UK
Tel. 44 923 663 331
Fax: 44 923 662 075

GREAT BASIN AERIAL
SURVEYS, INC.
5301 Longley Lane,
Suite 52, Reno
NV 89511
USA

GULF PETROLINK
P.O. Box 20393
Manama
Bahrain
Tel. 973 214881
Fax: 973 214475

HANSA LUFTBILD
GROUP
Elbestr. 5
Münster
Germany

HEWLETT-PACKARD
COMPANY
2000 West Loop South
Houston, TX 77027
USA
Tel. 713 439-5300
Fax: 713 439-5495

HOUSTON GEOSCAN,
INC.
Box 21849
Houston, TX 77218-
8849, USA
Tel. 713 579-8096
Fax: 713 579-6569

HSC SOFTWARE
1661 Lincoln Blvd.
Suite 101
Santa Monica
CA 90404
USA
Tel. 310 392-8441
Fax 310 392-6015

IBM CORP.
4800 Falls of the Neuse
Road, Raleigh
NC 27609
USA

IMAGE MAPPING
SYSTEMS
516 South 51 Street
Omaha, NE 68106
USA

IMAGE SCANS, INC.
4330 West 37th Ave.
Suite 100, Denver
CO 80212
USA

INSTITUT FüR RAUM-
INFORMATIONEN
Bahnhofstraße 20
Memmingen, D-87700
Germany

INTEGRATED MAP-
PING, LTD.
P.O. Box 2708
Christchurch
New Zealand

INTERNATIONAL
IMAGING SYSTEMS
2101 Business Ct. Dr.
Suite 130
Irvine, CA 92715
USA
Tel. 714 253-4612

INTERNATIONALES
LANDKARTENHAUS
Postfach 800830
Schockenriedstraße 44
Stuttgart 80, D-7000
Germany
Tel. 49 711 7 889 340
Fax: 49 711 7 999 354

SCIENTIFIC COMPUTER APPLICATIONS, INC.

Mapping-Contouring System

- *Always honors every data point.*
- *Makes maps that look hand-contoured.*
- *Contours up to 125 surfaces simultaneously.*
- *Handles multiple intersecting non-vertical faults among multiple surfaces.*
- *Merges seismic and geologic data.*
- *Creates rigorous multi-surface point-to-point cross sections.*
- *Integrates volumes rigorously, even in fault wedge areas.*
- *Prepares input for reservoir models and displays model results.*

Mapping-Contouring System (MCS) is a multi-surface geological/geophysical modeling system that can be applied to virtually any task: Geological, geophysical, environmental and mining. The system contours random or ordered data and always honors every data point regardless of clustering. MCS divides the map area into a system of triangles with a data point at each vertex. The original data points are retained throughout all subsequent processing, thereby insuring that all data points are honored. MCS runs on PC's or on workstations, and the maps look hand-contoured!

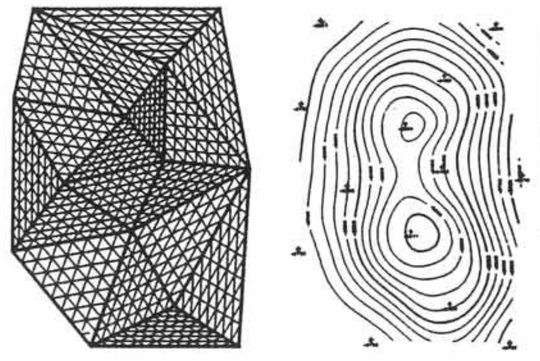

MCS Triangles **MCS Map**

Multi-Surface Contouring and Cross Sections

Mapping-Contouring System can contour one surface or many surfaces simultaneously, thereby making a number of structural maps and isochores at the same time. MCS first makes a series of isochore maps and interpolates or extrapolates these maps as necessary to cover the map area. Then these isochores are used to reconstruct missing values downward and upward in the stack so that at the end of the processing procedure there is a complete set of structure and isochore maps on all surfaces.

MCS *features*

- *Interfaces with AutoCAD and other CAD programs.*
- *Interfaces with SeisVision, GeoGraphix, SMT, GMA, and Paragon on PC's and with Landmark, GeoQuest, CogniSeis, and Vortext on Workstations.*

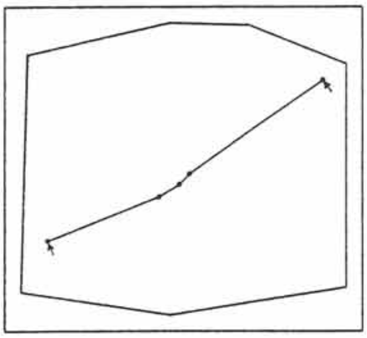

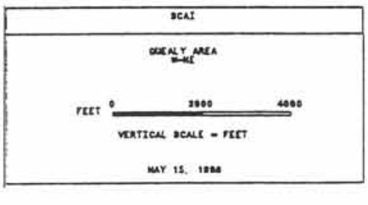

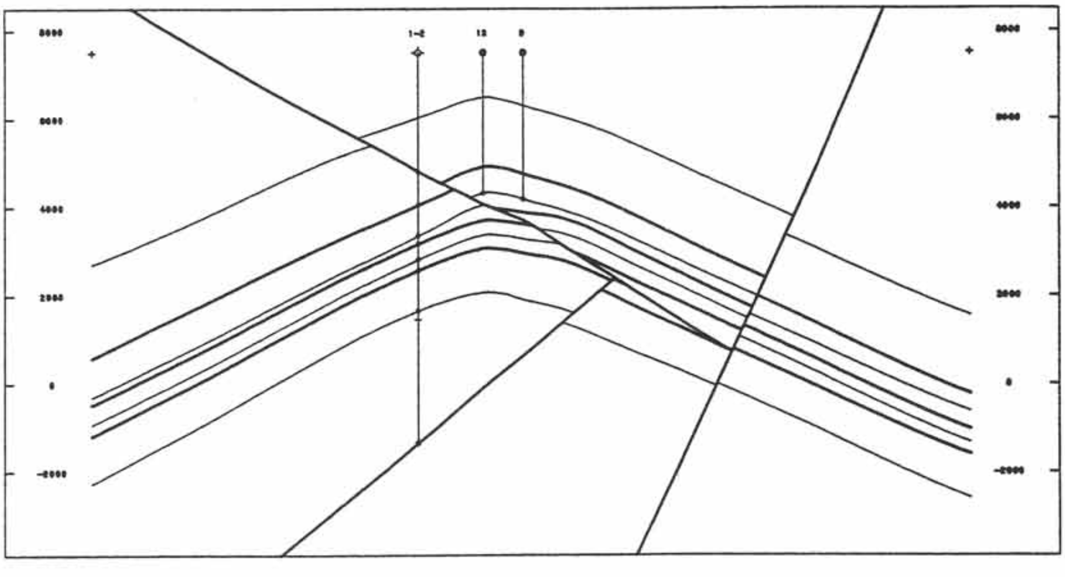

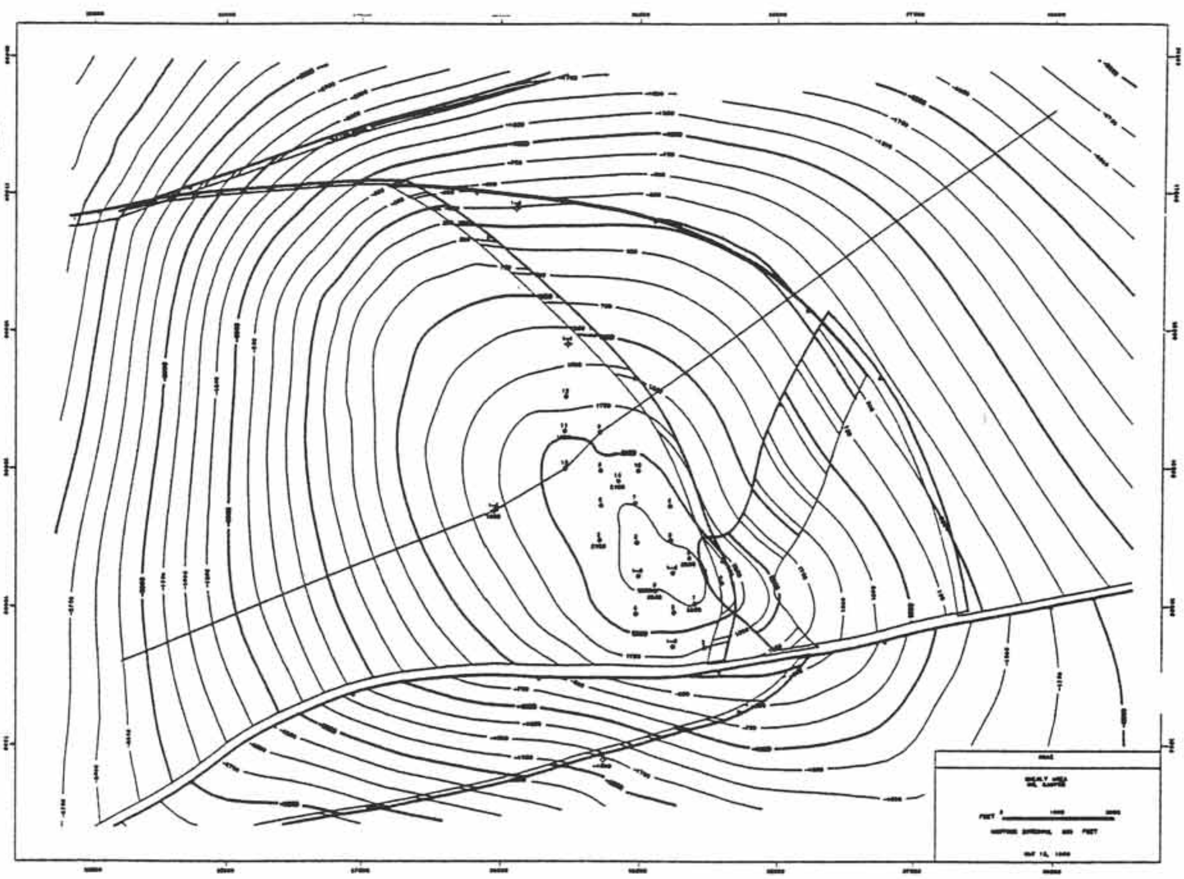

KEYSTONE AERIAL SURVEYS, INC.
P.O. Box 21059
Philadelphia, PA 19114
USA

LANDMARK GRAPHICS CORP.
15990 N Barkers Landing Rd.
Suite 100, Houston
TX 77079
USA
Tel. 713 584 5700
Fax: 713 589-9871

LARSON PLOTTING TECHNOLOGY
1111 Wilcrest Green Dr., Suite 225
Houston, TX 77042
USA
Tel. 713 977-4177
Fax: 713 977-4176

LEICA, INC.
2 Inverness Dr. E.,
Suites 106-108
Englewood, CO 80112
USA

LES SERVICES CARTOGRAPHIQUES 1 & 2
492 Blvd. de l'Hopital
Suite 101
Gatineau, PQ
Canada, J8V 2P4

LOGICA, INC.
32 Hartwell Avenue
Lexington
MA 02173-3103
USA
Tel. 617 476-8000
Fax: 617 476 8010

LOTUS DEVELOPMENT CORP.
55 Cambridge Pkwy.
Cambridge, MA 02142
USA
Tel. 800 635-6887
617 577-8500

LSU, REMOTE SENSING & GIS
E302 Howe-Russell
Geosci. Complex
Baton Rouge
LA 70803
USA

LYNX GEOSYSTEMS INC.
400-322 Water Street
Vancouver, BC
Canada, V6B 1B6

MAGELLAN SYSTEMS
960 Overland Court
San Dimas, CA 91773
USA

MAP SERVICES
5 Priory Road
Lower Compton
Plymouth, PL3 5EN
UK
Tel. 44 752 262 092

MAPA INT. GROUP
One Stuart Road
Thornton Heath
Surrey, CR7 8RA
UK
Tel. 44 81 665 0384

MAPCOM SYSTEMS
7345 Whitepine Road
Richmond, VA 23237
USA

MAPINFO CORP.
1 Global View
Troy, NY 12180
USA

MAPLINK
25 E Mason Street
Santa Barbara
CA 93101
USA

MAPPING AUTOMATION INC.
1100 E. University Dr.
Suite 114, Tempe
AZ 85281
USA

MAPPOWER CORP.
17 Main Street
Suite 313, Cortland
NY 13045
USA

MAPS GEOSYSTEMS
Corniche Plaza I
P.O. Box 5232
Sharjah
U. Arab Em.

MAPS GEOSYSTEMS
Truderinger Straße 13
Münich, 81677
Germany

MAPWARE A/S
P.O. Box 65
Lokkeveien 10
Stavanger, N-4001
Norway
Tel. 47 51 528 745
Fax: 47 51 529 135

MAPWARE CORP.
55-280 Metcalfe Street
Ottawa, Ontario
Canada, K1P 6L5

MICRO IMAGES, INC.
201 North 8th Street
Lincoln
NE 68508-1347
USA
Tel. 402 477-9554
Fax: 402 477-9559

MICROSOFT CORP.
One Microsoft Way
Redmond
WA 98052-6399
USA
Tel. 206 882-8080
Fax 206 93-MSFAX

NATIONAL REMOTE SENSING CENTRE
Delta House
Southwood Crescent
Southwood, Farnborough, Hampshire
GU14 0NL, UK
Tel. 44 252 541 464
Fax: 44 252 375 016

NEC TECHNOLOGIES, INC.
1414 Massachusetts Avenue
Boxborough
MA 01719-2298
USA
Tel. 508 264-8000
Fax: 508 263-3748

NEURALOG, INC.
2437 Bay Area Blvd.
Suite 414, Houston
TX 77058
USA
Tel. 800 364-8728

OGCI SOFTWARE, INC.
One Park Ten Place
Suite 150, Houston
TX 77084
USA
Tel. 713 579-2600
Fax: 713 579-2699

OMNI RESOURCES
1004 S. Mebane St.
P.O. Box 2096
Burlington, NC 27216
USA
Tel. 919 227-8300
Fax: 919 227-3748

ORDNANCE SURVEY OF IRELAND
Phoenix Park
Dublin 8
Irish Republic
Tel. 353 1 206 100
Fax: 353 1 204 156

PACIFIC INTERNATIONAL MAPPING
101-4218 Commerce Circle, Victoria
British Columbia
Canada, V8Z 6N6

PANGEA SCIENTIFIC, LTD. R.R. BOX 5
Brockville, Ontario
Canada, K6V 5T5

PAT DUNLAVEY CARTOGRAPHICS
40 Oblong Road
Williamstown, MT
01267
USA

PCI REMOTE SENSING CORP.
925 N. Lynn Street
Suite 803
Arlington, VA 22209
USA
Tel. 703 243-3700
Fax: 703 243-3705

PETRO CONSULTANTS
24 Chemin de la Marie
1258 Perly
Switzerland
Tel. 41 22721-1892
Fax: 41 22721-1894

PETROLEUM INFORMATION CORP.
4605 Post Oak Place
Suite 130, Houston
TX 77027
USA
Tel. 713 850-9295

PETROLEUM SOFTWARE SYSTEMS, INC.
7701 S Western
Oklahoma City
OK 73139
USA
Tel. 405 636-1587

PETROSCAN, AB
Kungsgatan 38-40
S-411 19 Göteborg
Sweden
Tel. 46 31 101 720

TNTlite™

For ten years, MicroImages has led the industry in developing and supplying advanced products for geospatial data analysis. Today the TNT professional products are used in 75 nations. Now, MicroImages makes the TNTlite version of the TNT products available at no cost. The free TNTlite products are restricted only in the size of the geodata sets they can use. They are identical to the TNT professional products in all other respects and are available for all popular networks and computer platforms: UNIX, Windows, or MacOS.

Why a free product?

The free TNTlite spatial data analysis products can provide a student anywhere in the world with a personal set of tools with which to learn the analytic techniques used with computer maps, images, and related geodata. In addition, TNTlite lets professionals in any discipline experiment with applications in new spatial data analysis technologies such as GIS, image processing, and relational imagery.

Where does geodata come from?

Growing collections of free geodata are available on the internet and are also appearing on low-cost CD's. You can get coverages for the world or for your particular locale and use the data immediately with TNTlite. For ten years TNT products have boasted the most extensive and up-to-date import capabilities for commercial and public domain geodata formats in the industry. You can import data directly, or link to external geodata files in many formats. The TNTlite products also support direct color image scanning, raster to vector line extraction, heads-up screen digitizing, and other geodata creation features. You can use all these approaches to acquire or create geodata sets for your local projects, class tutorials, or practice exercises.

What's the catch?

The TNTlite products are intended for the student who is using small data sets for a wide range of activities, from simple lab exercises to complex projects. TNTlite is not suited for those who are engaged in large projects or contracting for production work that requires large data sets. Thus, the primary difference between TNTlite and the professional TNT products is in the size limits MicroImages has placed on TNTlite geodata objects. For example, TNTlite limits each individual

raster (image) object to 512 by 512 pixels,
vector object to 500 polygons,
CAD object to 500 elements,
TIN object to 500 triangles, and
relational database tables to 1500 records.

Note: these size constraints do not limit the spatial extent of an object; you can enlarge the geospatial extent of an object by changing the scale or density of the elements in the object. Conversely, you can increase the small scale detail in an object by reducing its spatial extent.

How does TNTlite differ from a demo?

Within the size constraints of the geodata objects described above, TNTlite gives you unlimited access to all the processes and functionality of the TNT professional products. By contrast, a typical demo product may limit your evaluation period, or restrict access to some program features. TNTlite does not restrict you to demo data sets or to a single computer platform (use any Windows, Mac, or UNIX computer that has at least 16 Mb of memory). You can install TNTlite to your hard drive, or run it directly from the CD. You can have an unlimited number of geodata objects in your project files, and you can get free upgrades four times a year. You can even run TNTlite products over a network and use it from a remote site on any type of computer.

What's in it for MicroImages?

MicroImages has been in business for ten years developing and selling professional map and image processing products. We have created TNTlite as a unique abstraction of our professional TNT products so that anyone can use them without cost. We expect that some of you who acquire and refine new professional skills with TNTlite will eventually move up to our professional products. In the mean time, use TNTlite with our compliments for your projects, self-education, and professional advancement.

How do you get a free copy?

The TNTlite products for your computer can be downloaded anytime from MicroImages' home page at http://www.microimages.com. Consider however, that TNTlite uses exactly the same executables as the TNT professional products, and so the version for each platform takes approximately 100 megabytes. In addition, you will want at least some of the sample data. If your connection to the MicroImages web site is limited to modem speeds, you may judge a complete download to be impractical. As an alternative, you can order the current TNT Products CD for the cost of shipping and handling. Ordering the CD is a good idea if you have limited hard drive space, since the TNTlite products can run directly from the CD, saving 100 Mb of drive space.

AdvancedSoftwareforGeospatialAnalysis

MicroImages, Inc. • 201 North 8th Street • Lincoln, Nebraska • 68508-1347 USA
Voice (402) 477-9554 • FAX (402) 477-9559 • email info@microimages.com • internet http://www.microimages.com

PETROSYS, PTY., LTD.
58 Beulah Road, Unit 4
Norwood, SA 5067
Australia
Tel. 61 8 363 0922
Fax: 61 8 362 1840

PETROTECHNICAL
OPEN SOFTWARE
CORP.
10777 Westheimer
Suite 275
Houston, TX 77042
USA
Tel. 713 784-1880
Fax: 713 784-9219
E-mail: info@posc.org

PETROWARE SYS-
TEMS, INC.
5495 Beltline Road
Suite 150
Dallas, TX 75240
USA
Tel. 214 490-4931
Fax: 214

PGS RESERVOIR
11200 Westheimer
Suite 200, Houston
TX 77042
USA

PHOTO MARKETING
ASSOCIATION INT.
3000 Picture Place
Jackson, MI
USA
Tel. 800 248-8804
517 788-9100
Fax: 517 788-8371

PHOTO SCIENCE, INC.
45 West Watkins Mill
Road, Gaithersburg
MD 20878
USA

PHOTOTHEQUE NATIO-
NALE
2, Avenue Pasteur
94160 St. Mande, Paris
France

PINNACLE MICRO
19 Technology
Irvine, CA 92718
USA
Tel. 800 553-7070
714 727-3300
Fax 714 727-1913

POLAROID Co.
549 Technology SQ
Cambridge, MA 02139
USA

PRAKLA-SEISMOS AG
Buchholzer Str. 100
P.O. Box 510530
D-3000 Hannover 51
Germany
Tel. 511 6420
Fax: 647 6860

PROJECTIONS MAP-
PING GROUP, INC.
900-6 Avenue S.W.
Suite 350
Calgary, Alberta
Canada, T2P 3K2

RAISZ LANDFORM
MAPS
P.O. Box 773
Melrose, MA 02176
USA
Tel. 800 242-3199
Fax: 617 662-2622

REMAP CORP.
774 Transfer Road
St. Paul, MN 55114
USA

REMOTE SENSING
APPLICATIONS
Monks Wood
Abbots Ripton
Huntingdon
Cambridgeshire
PE17 2LS, UK
Tel. 44 4873 381/8
Fax: 44 4873 467

REMOTE SENSING
SOCIETY
University
of Nottingham
Nottingham, NG7 2RD
UK
Tel. 44 602 515 435
Fax: 44 602 515 249

REPROCART, B.V.
Ceintuurbaan 213A
3051 KC Rotterdam
Netherlands

ROCKWARE, INC.
Rockware Building
2221 East Street
Suite 101, Golden
CO 80401
USA
Tel. 303 278-3534
800 775-6745
Fax: 303 278-4099

SILICON GRAPHICS
Forum 1, Station Road
Theale
Reading, RG7 4RA
UK
Tel. 44 734 306 222
Fax: 44 734 302 550

SPACE IMAGING
9351 Grant Street
Suite 500
Thornton, CO 80229
USA

SPOT IMAGE
5, Rue des Satellites
Toulouse, 31030
France

SPOT IMAGE CORP.
1897 Preston White
Drive, Reston
VA 22091-4326
USA
Tel. 703 620-2200

STRATAMODEL, INC.
7500 San Felipe
Suite 500
Houston, TX 77063
USA
Tel. 713 781-5119
Fax: 713 781-5136

STRATEGIC MAPPING,
INC.
3135 Kifer Road
Santa Clara, CA 95051
USA

SUBSURFACE COM-
PUTER MODELING
3103 Bee Caves Road
Suite 133
Austin, TX 78746
USA

SURVEYING AND MAP-
PING AGENCY NRW.
Muffendorfer Straße
19-21, Bonn 2
53177 Germany

TANDY CORP.
One Tandy Center
Fort Worth, TX 76102
USA
Tel. 817 390-3700

TASA GRAPHIC ARTS
11930 Manaul Blvd.
NE, Suite 107
Albuquerque
NM 87112-2461
USA

TECHLOGIC
15325 189th Ave. NE
Woodinville
Washington DC
USA

TEKTRONIX, INC.
P.O. Box 1000
MS 60-787
Wilsonville, OR 97070
USA

TEKWARE, LTD.
Worcester Road
Hagley, West Midlands
DY9 ONW
UK
Tel. 44 562 882 125
Fax: 44 562 884 855

TERRA SURVEYS, LTD.
2060 Walkley Road
Ottawa, Ontario
K1G 3P5, Canada

TERRA-IMAGE
1100 Geomap Lane
Plano, TX 75074-7199
USA
Tel. 214 578-0571
Fax: 214 424-5533

TERRASCIENCES
2901 Wilcrest
Suite 350
Houston, TX 77042
USA
Tel. 713 861-0392

TERRATECH MAPPING
SERVICES, INC.
206-5050 Kingsway
Burnaby, British Colum-
bia
V5J 1T1, Canada

TEXAS INSTRUMENTS,
LTD.
m/s 24, Manton Lane
Bedford, MK41 7PA
UK
Fax: 0234 22 3167

THE GEOLOGICAL
SOCIETY OF AMERICA
3300 Penrose Place
P.O. Box 9140
Boulder, CO 80301
USA
Tel. 303 447-2020
Fax: 303 447-1133

THE HYPERMEDIA GROUP
5900 Hollis Street,
Suite O, Emeryville
CA 94608
USA
Tel. 415 601-0900
Fax 415 601-0933

TNO INSTITUTE OF APPLIED GEOSCIENCE
P.O. Box 6012
2600 JA Delft
Netherlands
Tel. 31 15 697 197
Fax: 31 15 564 800

TOPOGRAPHIC ENGINEERING CO.
6709 N Classen Blvd.
Oklahoma City, OK 73116
USA
Tel. 405 843-4847
Fax: 405 843-0975

TOSHIBA AMERICA
P.O. Box 19724
Irvine, CA 92713
USA
Tel. 714 583-3000

TRIPLE POINT SOFTWARE
1107 Fair Oaks Avenue #121
S. Pasadena
CA 91030
USA
Tel. 818 441 9745
FAx: 818 441 1048

UNISYS
13430 Northwest Fwy., Suite 500
Houston, TX 77040
USA
Tel. 713 744-2666

UNITED AERIAL MAPPING, INC.
5411 Jackwood Drive
San Antonio, TX 78238
USA

USER SERVICES EARTHNET
Via Galileo Galilei
C.P. 64, 00044 Frascati
Italy

USGS, NATIONAL CARTOGRAPHIC CENTER
507 National Center
Reston, VA 22092
USA

VIRTUAL REALITY LAB'S, INC.
2341 Ganador Court
San Luis Obispo
CA 93401
USA
Tel. 805 545-8515
Fax 805 545-8515

WEST AIR
49 Birnbeck Road
Anchor Head
Weston-Super-Mare
Avon, BS23 1QZ
UK
Tel. 44 860 710 233
Fax: 44 934 635 421

WESTERN AERIAL PHOTOGRAPHY LAB.
P.O. Box 30010
Salt Lake City
UT 84115
USA

WESTERN ATLAS SOFTWARE
Box 1407, Houston
TX 77251-1407
USA
Tel. 713 972-4600
Fax: 713 972-4599

WESTERN GEOPHYSICAL
1001 Richmond Ave.
Houston
TX 77042-4299
USA
Tel. 713 963-2500
Fax: 713 963-2030

WORLD DATA CENTER FOR ROCKETS
Goddard Space Flight Center, Greenbelt
MD 20771
USA

Z & S GEOLOGI A.S.
Sverdrupsgate 23
Stavanger, N-4007
Norway
Tel. 47 4 52 2965
Fax: 47 4 52 2985

Alboran's Lectures in Geoscience is a textbook series, prepared by experienced earth scientists. The lectures are carefully organized and balanced in approach. Many professionals, students, and instructors have discovered the practical value of these books as user-friendly instruction manuals.

By way of introduction

The discipline of *structural geology* studies the architecture of the solid Earth and other planets. Rock deformation patterns are exciting features because of their aesthetic beauty and their economic interest to man. Knowledge of the subsurface structure is vital for the success of a variety of engineering and mineral exploration programs. A thorough understanding of rock structures is essential for strategic planning in the petroleum and mining industry, in construction operations, in waste disposal surveys, and for water exploration. Deformation structures in the country rock are important further for localizing hazard zones, such as potential rockslide masses, ground subsidence, and seismic faults. Research activities concentrate on rock deformation structures in the shallow continental crust.

Structural Geology and Map Interpretation is designed for undergraduate students in civil engineering, petroleum engineering, mining technology, hydrology, environmental studies, geophysics, and geology. The principles of structural geology are carefully introduced and systematically developed, accompanied by instructive illustrations and penetrative exercises on map interpretation. This state-of-the-art account covers one semester of teaching and helps to establish a streamlined communication between students and their instructors, providing common language on the techniques and principles of structural geology. Because the theory is combined with practical exercises, this book may be used for both lectures and laboratory sessions. Using a single textbook, comprising two integrated packages, rather than two separate books is practical and keeps the cost affordable for students.

Alboran Science Publishing Ltd. publishes high-quality textbooks, research books, conference proceedings, and journals of scientific merit. The adoption of new titles is subject to rigorous assessments by experts. Alboran is primarily interested in publishing work in the field of the earth sciences. For more information, please contact the *Publications Manager, Mr. J. Outhuis, Laurierstraat 132A, Amsterdam 1016 PR, the Netherlands. Fax: + 31 20 364 0145.* For details on book ordering procedures, please consult the instructions on the separate order form accompanying this book or contact Alboran's sales office.

ISBN 90-5674-001-6

ISBN 90-5674-001-6

SCIENCE Alboran

9 789056 740016